Mid-Infrared Laser Applications in Spectroscopy

Frank K. Tittel[1], Dirk Richter[2], and Alan Fried[2]

[1] Rice Quantum Institute, Rice University
Houston, TX 77251–1892, USA
fkt@rice.edu

[2] The National Center for Atmospheric Research
1850 Table Mesa Dr., Boulder, CO 80305, USA
{dr,fried}@ucar.edu

Abstract. The vast majority of gaseous chemical substances exhibit fundamental vibrational absorption bands in the mid-infrared spectral region ($\approx$ 2–25 µm), and the absorption of light by these fundamental bands provides a nearly universal means for their detection. A main feature of optical techniques is the non-intrusive *in situ* detection capability for trace gases. The focus time period of this chapter is the years 1996–2002 and we will discuss primarily CW mid-infrared laser spectroscopy. We shall not attempt to review the large number of diverse mid-infrared spectroscopic laser applications published to date. The scope of this chapter is rather to discuss recent developments of mid-infrared laser sources, with emphasis on established and new spectroscopic techniques and their applications for sensitive, selective, and quantitative trace gas detection. For example, laboratory based spectroscopic studies and chemical kinetics, which will also benefit from new laser source and technique developments, will not be considered.

1 Solid-State Mid-IR Spectroscopic Laser Sources

Mid-infrared laser sources come in many different varieties. For their application to spectroscopic measurement, and specifically for quantitative measurements, the ideal source would have the following properties: (1) sufficient optical power to overcome inherent electronic detection noise and ensure high laser signal-to-noise ratios, (2) narrow linewidth to obtain high selectivity and sensitivity, (3) single longitudinal mode operation with low amplified spontaneous emission output for high selectivity and elimination of intermode competition noise; (4) ease of tailoring the inherent laser operating wavelength (design of gain material and/or cavity structure) to access the desired absorption region; (5) low source noise and low amplitude modulation; (6) high beam quality, i.e., small beam divergence, small astigmatism, and stable, predictable beam output direction, for optimum coupling into and through a gas sampling cell; (7) low temperature and current tuning rates to minimize wavelength jitter induced by controller noise; (8) rapid wavelength tunability for fast response and high data acquisition rates; (9) minimal susceptibility to changing environmental conditions of temperature, pressure, humidity,

I. T. Sorokina, K. L. Vodopyanov (Eds.): Solid-State Mid-Infrared Laser Sources,
Topics Appl. Phys. **89**, 445–516 (2003)

and vibrations; (10) no long term changes in laser wavelength and/or spatial output characteristics; (11) highly reliable performance for many years; and (12) compact and robust overall sensor package size. Of course it is challenging to realize all these idealized attributes in any one real world mid-infrared laser source, and they are listed here to serve as a general guideline. However, some of the attributes are more important than others for a given application to obtain the best possible measurement performance. In the sections that follow, we will elucidate wherever possible those important attributes necessary for achieving optimal performance employing the technique being discussed.

It is common practice in infrared spectroscopy to express transition frequencies in inverse centimeters (cm^{-1}), or *wavenumbers*, defined simply as the inverse of the transition wavelength in vacuum, $\nu = \lambda^{-1}$. Multiplying this quantity by c gives the frequency in hertz; thus $1\,\mathrm{cm}^{-1}$ is roughly 30 GHz. We shall use both units throughout this chapter, where appropriate.

The spectral coverage of the most frequently employed tunable CW mid-infrared sources is shown in Fig. 1. In general, one can distinguish between two classes of mid-IR laser sources. Class "A" includes sources which generate tunable mid-IR laser radiation directly from gain in gas discharge, semiconductors, rare-earth and transition-metal doped solid-state bulk materials or optical fibers. Class "B" laser sources are based on nonlinear optical parametric frequency conversion of near-infrared ($\approx$ 0.9 to 2 µm) laser sources.

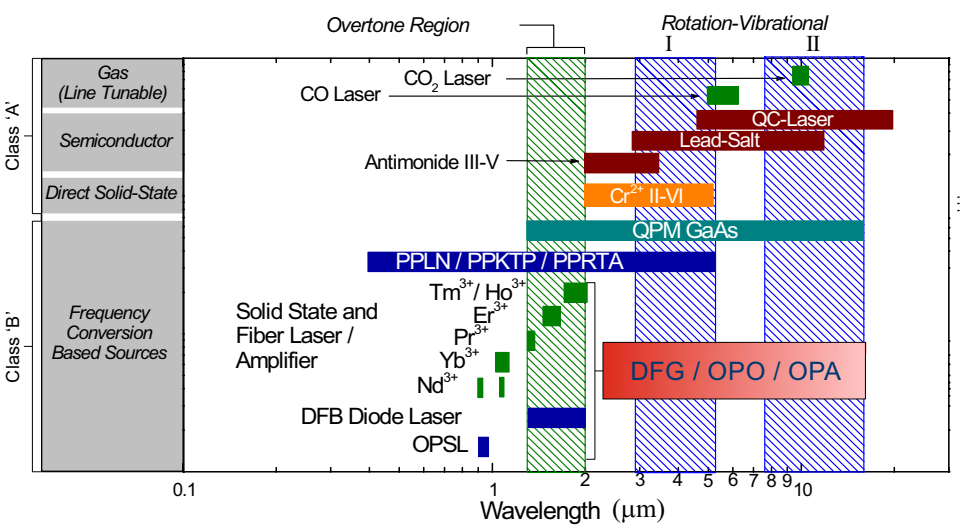

Fig. 1. Laser sources and typical wavelength coverage. Shown are also the wavelengths of the two atmospheric windows I (2.9 –5.3 microns) and II (7.6–16 microns), typically accessed for trace gas sensing. OPSL, optically pumped semiconductor laser

Many hundreds of non-linear optical crystals have been developed for this purpose, however only very few of these are practical and in use. In this chapter, examples of parametric frequency conversion sources will be limited to quasi-phase-matched materials (QPM). While class "A" mid-IR laser sources are inherently more compact, class "B" laser sources can be made to operate over a much wider wavelength spectrum, often in a single optical arrangement, which is a key advantage for certain applications. Figure 1 shows the spectral coverage of Class "A" and "B" laser sources in the mid-IR wavelength region. The merits of the various spectroscopically important laser sources shown will be discussed in this section. Although line-tunable laser sources such as CO and CO_2 gas lasers have and are being successfully used in trace gas detection [1,2], they are not within the scope of this book, which focuses specifically on solid-state laser sources.

1.1 Class "A" Laser Sources

Class "A" lasers as defined above, are direct laser sources. In the following subsections these lasers are discussed with respect to their typical operating characteristics and optical set-up conditions. The first group of class "A" lasers is further subdivided into semiconductor based lasers, namely lead-salt, antimonide and quantum cascade laser sources, which share some common features such as cryogenic cooling (in some cases thermoelectric) and the set-up of collection optics. This section is followed by a discussion of tunable solid-state laser sources.

1.1.1 Lead-Salt Diode Lasers

Lead-salt diode lasers have been developed for operation at wavelengths from 3 to 30 μm and have been available since the mid-1960s. These lasers are comprised of PbTe, PbSe, and PbS and various alloys of these compounds with the same materials above and with SnSe, SnTe, CdS and other materials. The lead-salt diode laser consists of a single crystal of these semiconductor materials to form a p–n junction. The crystal is shaped into an optical cavity employing parallel end faces that are approximately 250 μm square at both the front and rear faces. Typical cavity lengths range from ≈ 300 to 500 μm. Lasing action is achieved by applying a forward bias current which injects charge carriers (electrons or holes) across the p–n junction, and this in turn populates the nearly empty conduction band. Stimulated emission across the band gap between the conduction and nearly full valance band provides the gain mechanism for lasing action. Since the emission photon energy approximately equals the band gap energy, which in the case of Pb-salt materials is small, these lasers require cryogenic cooling to achieve population inversion. These lasers therefore are subject to temperature extremes (≈ 10–300 K) and this places stringent demands on the entire laser package.

The energy band gap, which is dependent upon semiconductor composition and crystal temperature, determines the output lasing wavelength. One can tailor the lasing wavelength regime at the time of manufacture by either varying the stoichiometry between Pb and the other constituents or by employing different alloys of Pb. Any given device can be actively tuned in wavelength over $\approx 100\,\mathrm{cm}^{-1}$ by changing the device temperature, or over tens of cm^{-1} by changing the injection current. Both tuning mechanisms, however, produce semicontinuous wavelength coverage, since the laser structure is a Fabry–Pérot device. Varying the injection current generally allows continuous tunability over a ≈ 1–$2\,\mathrm{cm}^{-1}$ spectral region before the output jumps to a new longitudinal mode. In some cases the gain is broad enough to support multiple longitudinal modes simultaneously, resulting in wavelength regions where the lasing output gradually shifts from one mode to another. Tuning by temperature takes advantage of the change in band gap, and hence the wavelength with temperature. Typical rates range between 2 and $5\,\mathrm{cm}^{-1}/\mathrm{K}$. Since this mechanism involves changing the temperature of the entire laser package, including the stage on which the laser is mounted, temperature tuning is very slow on the order of seconds. Since typical absorption linewidths are in the $0.001\,\mathrm{cm}^{-1}$ range, at reduced pressures of several tens of Torr typically employed in sample cells, stable operation requires temperature control to better than 1 mK over long time periods. Tuning by current, which involves ohmic heating of the active region only, causes a change in the refractive index of this region, which in turn produces a change in wavelength. This tuning mechanism is very rapid, thus making it possible to employ high frequency modulation techniques in the kHz to MHz regime. Typical current tuning rates range between 0.02 and $0.07\,\mathrm{cm}^{-1}/\mathrm{mA}$ (≈ 606–$2121\,\mathrm{MHz}/\mathrm{mA}$). This rapid tuning mechanism, however, also requires low noise laser current controllers in order to avoid linewidth broadening. Given the typical absorption linewidths above, low noise controller operation of $10\,\mu\mathrm{A}$ or better is required. Employing such a low noise temperature and current controller, *Reid* et al. [3] determined that the measured linewidths from Pb-salt diode lasers varies dramatically from laser to laser, and for any given laser, depends strongly upon the junction temperature and injection current. Typical linewidths (FWHM), in the absence of refrigerator shocks caused by the closed cycle cooling system employed, were 0.6–25 MHz. Vibrations from the closed cycle cooler degraded this linewidth to $\approx 60\,\mathrm{MHz}$. However, linewidths of $\approx 100\,\mathrm{MHz}$ or more were sometimes observed by *Reid* et al. and by *Lundqvist* et al. [4]. *Sams* and *Fried* [5] discussed the effect of such mechanical vibrations on quantitative spectroscopic determinations. Since most diode lasers now operate at or above liquid nitrogen temperatures, where liquid nitrogen dewars have replaced closed cycle refrigerator systems, one should expect linewidths $\leq 25\,\mathrm{MHz}$.

Older Pb-salt devices were grown by a diffusion process, which unfortunately often resulted in a poorly defined lasing region. In many instances

lasing occurred over nearly the entire junction width in multiple filaments, which in some cases produced a laser output in different directions with different wavelengths [6]. Even when such multiple beams were not present, the main emission lobe was sometimes emitted at an angle relative to the optic axis of the laser. The resulting poor spatial beam quality, which made it extremely difficult to optimally collect the output beam, together with other problems just discussed, has no doubt contributed to the poor performance reported by many early users of Pb-salt devices. This has led to the development of newer Pb-salt lasers based on mesa structure and ultimately buried heterostructure or double heterostructure devices in which the active lasing area is highly confined to a region less than 1 μm thick and less than 10 μm wide. These devices, which are discussed by *Preier* et al. [7], are prepared by molecular beam epitaxy using PbEuSeTe or PbSnTe active layers. In addition to improved output beam quality, which as we will show is very important for trace gas detection employing multi-pass absorption cells, these newer devices exhibit threshold currents as low as 1 mA and higher operating temperatures. Most of these devices typically operate at temperatures between 77 and 120 K, which is accessible using liquid nitrogen cryogenic dewars instead of bulky and noisy closed cycle refrigerator systems required by earlier devices. Despite this significant effort, Pb-salt diode lasers have not been manufactured to routinely operate CW at temperatures much higher than the above range and certainly less than the highest reported temperature of 215 K for CW operation published by *Wall* [8]. Typical CW single mode output powers for Pb-salt lasers are in the range 100–500 μW. For comprehensive reviews of Pb-salt diode lasers, their electrical and optical properties, performance characteristics and device materials along with the corresponding manufacturing techniques, the reader is referred to [7,8,9], and the many references found in *Grisar* [10]. Brassington also presents an excellent review of these topics as well as applications of Pb-salt lasers [11].

Unfortunately due to the small market for Pb-salt lasers, significant advances in device structure based on buried quantum well, distributed feedback and distributed Bragg reflectors, which appeared so promising in the 1990s, are not being aggressively pursued at present. Since lead-salt diode lasers can be modulated at very high frequencies (tens of kHz up to several hundred MHz), similar to those of near-infrared diode lasers, harmonic detection and two-tone modulation techniques can be employed as an efficient means of reducing noise (Sect. 1.2.2). As discussed previously, all CW Pb-salt diode lasers require some form of cryogenic cooling for operation. Although cryogenic operation is feasible and indeed commonplace in field environments, even in rugged airborne laser systems [12], such operation may impose limitations that can ultimately affect system performance. For example, all cryogenically cooled lasers are temperature cycled many times over their lifetime and may result in unrecoverable changes of the lasing frequency [13]. Other effects include long-term changes of tuning characteristics, slight changes of the

spatial mode quality, and reduction in laser power. Although all present Pb-salt devices are temperature-cycled by the manufacturer to minimize these problems, the finite possibility of such changes is disconcerting in certain demanding applications where it is imperative to access routinely a specific absorption feature. Airborne measurements of formaldehyde, where there is a limited choice of strong and interference-free absorption lines, is one such example [14,15]. In addition, since liquid nitrogen dewars frequently contain as many as four lasers, one runs the risk of mechanically disturbing all lasers in changing out any given laser. Small manipulations to the laser lead wires, which are unavoidable in this procedure, may result in irreversible changes to laser performance, similar to that from temperature cycling.

Lead-salt diode lasers also exhibit large beam divergence and astigmatism, which places critical and stringent alignment requirements on the collection optics, particularly the first optical element, which is placed in front of the dewar. Subtle changes in the alignment between the laser and the first collection optic, due to small mechanical changes in the position of either the laser or the optical element, necessitates periodic adjustments to the first collection element, and this may add some mechanical instability to the alignment. Such instability, even when relatively small, in turn often leads to optical noise in IR absorption systems. This noise source, which is produced by unwanted scattering off various optical elements, results in a periodically undulating background structure of varying amplitude, spacing, and temporal frequency.

Despite these drawbacks of lead-salt diode lasers, spectrometers employing these sources still yield excellent sensitivity, even in rugged field environments. As we will show in a later section, a liquid-nitrogen cooled Pb-salt diode laser spectrometer can routinely measure ambient formaldehyde (CH_2O) levels as low as 20–50 parts-per-trillion by volume (pptv) on an airborne platform employing 1-minute integration [16]. This corresponds to a minimum detectable absorbance, $A_{\min}$, of 0.7 to 1.7×10^{-6} (S/N = 1) using a 100-meter absorption pathlength.

Table 1. Summary of lead-salt diode laser characteristics

Wavelength range (μm)	Tuning (coarse/fine)	Power (mW)	Linewidth	Beam profile characteristics	Operating requirements
3–30	$100\,\mathrm{cm}^{-1}$/ $1\text{–}2\,\mathrm{cm}^{-1}$	0.1–0.5	1–1000 MHz	– Elliptical – Highly astigmatic – Highly divergent	Cryogenic cooling

1.1.2 Antimonide Diode Lasers

Continuous wave lasing at room temperature at wavelengths above 2 μm with output optical powers up to 20 mW/ facet has been achieved using structures grown by molecular beam epitaxy (MBE) on GaSb substrates

and employing compressively strained GaInSbAs quantum wells (QWs) between Ga(Al)Sb(As) barriers in the active region. Narrow ridge Fabry–Pérot GaInSbAs/GaSb type II electrically pumped QW lasers emitting at 2.35 μm have been reported [17,18]. For further details on mid-infrared heterojunction lasers see the chapter by Joullié et al. These lasers emit in a fundamental spatial mode and exhibit single frequency operation over a range of currents and temperatures. They emit in a spectral region where overtone and combination absorption lines of such gases as CO, CH_4, NH_3 and NO_2 can be accessed conveniently. In efforts to extend coverage to the fundamental spectral region, several groups have reported the development of antimonide diode lasers in the 2–3 μm spectral range [19] and InAsSb/InAs lasers between 3 and 5 μm [20,21,22,23,24]. However, this technology is not yet robust and single frequency operation by means of DFB (Distributed Feedback) laser designs has not been realized. Hence these devices must be operated in an external cavity configuration to achieve stable and narrow-linewidth operation. Although room-temperature operation has been demonstrated, reliable single-frequency operation still requires cryogenic cooling.

Table 2. Summary of antimonide diode laser characteristics

Wavelength range (μm)	Tuning (coarse/fine)	Power (mW)	Linewidth	Beam profile characteristics	Operating requirements
2–3; 3–5	1–2 cm^{-1}	0.1 (single-mode)	50 MHz	– Elliptical – Astigmatic – Highly divergent	– Thermoelectric (2–3 μm) – Cryogenic cooling (> 3 μm)

1.1.3 Quantum Cascade Lasers

Quantum cascade (QC) lasers are unipolar semiconductor injection lasers based on intersubband transitions in a multiple quantum-well heterostructure. They are designed by means of band-structure engineering and grown by molecular beam epitaxy. The emission wavelength of a QC laser depends on the thickness of the quantum well and barrier layers of the active region rather than the band gap of diode lasers. These lasers operate either as CW or pulsed devices. The chapter by Hofstetter and Faist as well as several papers in [25,26,27,28] provide details of their design and operating characteristics. In the following, an overview will be given on emission wavelengths, output powers and design approaches.

Quantum cascade lasers grown in a InGaAs/AlInAs lattice matched to the InP material system have been fabricated for emission wavelengths from 3.5 to 24 μm. Quantum cascade lasers have excellent spectroscopic properties in terms of optical power, but their tuning range is limited and their beam divergence is large and astigmatic. Multi-mode devices with 100 stages (quantum

well gain regions in series) have demonstrated peak powers of 0.6 W at room temperature. Until recently room temperature operation was only feasible for pulsed operation, but CW multi-spectral mode operation up to temperatures of 312 K was reported for a Fabry–Pérot style QC laser in 2002 [29]. Reliable single frequency operation has been achieved through the integration of a Bragg grating into the laser waveguide, resulting in a distributed feedback (DFB) laser, operating at cryogenic temperatures. The latest generation of QC-DFB lasers is based on a "top-grating" approach that takes advantage of the characteristics of a mid-infrared waveguide. For mid-infrared wavelengths below 15 μm, dielectric waveguides built from low-doped semiconductor layers that have appropriate refractive index modulation are used [30]. At longer wavelengths, the waveguide is overlaid with metal. In this case the radiation is guided not only by the dielectric but also by a surface plasmon mode [31].

Continuous wavelength tunability without mode hops is achieved through the temperature dependence of the waveguide parameters. The temperature can either be varied by a temperature change of the heat sink on which the device is mounted or more rapidly by dissipative heating through changing the direct QC laser excitation current. Characteristic total tuning ranges per current sweep are typically around 0.4 % of the emission wavelength. For many spectroscopic purposes, the spectral linewidth of the laser emission is as important as continuous tunability. The linewidth of selected CW DFB QC lasers ranges from a few MHz [32] through current stabilization to a few kHz with frequency stabilization [28], but exceeds 150 MHz (HWHM) in pulsed operation. Device reliability and long-term wavelength tuning characteristics are excellent as a result of using robust materials, such as InP and GaAs based heterostructures. To achieve mode-hop free tuning for Fabry–Pérot-type QC lasers in the mid-IR, a grating-coupled external cavity has been used to obtain a wavelength tuning of hundreds of nanometers, or up to 8 % of the central wavelength in the 3–4 μm region for InAs/InAsSb or GaSb/InAsSb heterostructure lasers with a few hundred milliwatts (mW) peak power [33]. Fabry–Pérot QC lasers [34] at 4.5 and 5.1 μm have been tuned with an external cavity. The principal technical issue is the need to deposit a low loss broadband antireflection coating or an angled surface on one of the laser output facets.

A practical consideration of QC lasers is their operating current requirements, often drawing multiple amperes of current in CW operation. In addition, a QC laser typically requires compliance voltages of 5–10 V. The resulting thermal load to the laser is significant and good thermal management is important to achieve room-temperature operation. Low noise drivers have been developed based on the modified Libbrecht design [35]. The use of batteries also permits low noise operation of QC lasers and linewidths below 1 MHz are obtained without frequency locking.

To date, QC laser-based chemical sensors primarily use InGaAs/InAlAs type-I QC-DFB devices. There are two limitations inherent to this kind of

Table 3. Summary of quantum cascade laser characteristics

Wavelength range (μm)	Tuning (coarse/fine)	Power (mW)	Linewidth	Beam profile characteristics	Operating requirements
4.3–24 (Selected regions where single-frequency operation has been demonstrated)	$35\,cm^{-1}$ with external grating cavity/ $3\,cm^{-1}$	1–100 (CW, single frequency) 50 (avg., pulsed)	0.001–10 MHz, CW (locked–unlocked) > 150 MHz (HWHM), pulsed	– Elliptical – Astigmatic – Highly divergent	– Cryogenic cooling (CW) – Peltier cooling (pulsed) – High voltage, high current low noise driving electronics

laser for chemical sensing. First, they cannot access the spectral region of C–H and O–H stretch vibrations near $3000\,cm^{-1}$. This shortcoming can be overcome by developing QC lasers based on alternative materials and structures. For example, the $3000\,cm^{-1}$ region is accessible by type-II lasers [36], but no single frequency devices of this kind have yet been demonstrated. Another issue is the limited tunability of each QC-DFB laser, which restricts the feasibility of multi-component chemical sensing. This requirement can be addressed by separating the gain medium from the wavelength-selective element [34,37]. In [34], a QC laser tunability of $\approx 35\,cm^{-1}$ at a fixed temperature was demonstrated in an external cavity configuration with a diffraction grating. This is about a ten times wider range than that typically achieved for QC-DFB lasers by means of current tuning. On-line concentration measurements of ≈ 20 gaseous compounds and several isotopomers in ambient air have been realized in the first three years of various QC laser based chemical sensors.

Mid-infrared semiconductor laser sources as discussed above share several common characteristics. Low temperature operation is yet the most reliable means of obtaining CW tunable single frequency emission. For the purpose of applying the generated radiation to a specific spectroscopic technique and application, the laser radiation has to be collected and mode matched to the spectroscopic sampling path or cell. Semiconductor lasers exhibit a large divergence and astigmatism and four representative approaches for beam collection, shaping and delivery to the spectroscopic sampling path are illustrated in Fig. 2.

Illustrated in Fig. 2a is the approach used by *Fried* et al. [16]. Here, all reflective elements are used to collect, collimate and image the laser radiation to a long-path absorption cell. Fig. 2b shows the approach used by *Nelson* [38], in which an all-reflective objective is used for the same purpose. However, collection efficiency is typically lower than the technique depicted in Fig. 2a due to center mirror obscuration by as much as 20 %. Care must be taken to avoid residual feedback of the center mirror, which may increase the laser noise and at times induce mode-hopping. In approach 2c (Laser Components, Inc.), a toroidal mirror is used as a first collection element to correct the astigmatism/emission aspect ratio and lower the divergence of

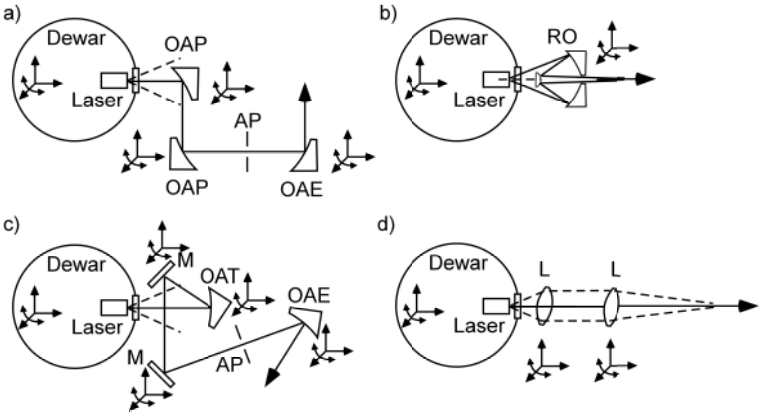

Fig. 2. Representative approaches for optical beam collection, shaping and imaging of highly divergent, astigmatic laser radiation. See text for explanation of figures. OAP, off-axis parabolic mirror; OAE, off-axis ellipsoidal mirror; AP, aperture; RO, reflecting objective; M, mirror; OAT, off-axis toroidal mirror; L, lens

the beam. An OAE re-images the beam to the sampling path or cell. This design provides a well-defined beam shape and quality, however at the cost of complexity and the use of four optical elements, all subject to drift, which can lead to beam pointing instabilities. The advantage of this configuration is that the beam can be optimally collected while maintaining a fixed output axis. The approach shown in Fig. 2d uses two lenses to collimate and re-image the laser [39], avoiding the spherical aberrations introduced by OAP and OAEs. Similar to the approach shown in Fig. 2b, feedback may be an issue to the laser wavelength stability and is subject to creating stronger optical interference fringes between refractive optical elements.

1.1.4 Tunable Solid-State Lasers

A large and important class of tunable lasers is based on the vibronically broadened transitions that can occur in certain gain media, such as color centers and certain transition metal or rare-earth ions in crystalline hosts [40,41,42,43]. When such a medium is placed in a tunable cavity and pumped above laser threshold, stimulated emission can be made to occur at any desired frequency within the emission band. Tunable laser media based on 3d–3d transitions of transition-metal ions and 4f–5d transitions of rare-earth ions cover the mid-infrared spectral range between 1.0 µm and 4.7 µm. The tuning range of such lasers can be widely varied by the choice of impurities and by selecting different hosts. Recent spectroscopic studies demonstrated that chromium-doped zinc selenide chalcogenides, such as Cr^{2+}:ZnSe and Cr^{2+}:ZnS, have favorable characteristics as tunable mid-infrared solid-state materials near 2.5 µm [44,45]. These include room-temperature operation,

broad tunability, the possibility of direct diode-pumping, erbium fiber amplifier and CW operation.

Table 4. Summary of tunable solid-state laser characteristics

Wavelength range (μm)	Tuning (coarse/fine)	Power (mW)	Linewidth	Beam profile characteristics	Operating requirements
2–5	600 nm/ 1 cm^{-1}	200–1000 → 20 →	800 MHz, 1 s 0.1 MHz, 1 s	– TEM_{00} – Cavity subject to pointing instability	Low technical noise environment

For selective spectroscopic detection at reduced pressures, the output power of the above mentioned solid-state laser sources is significantly reduced if one or more frequency selective optical elements are employed to obtain laser linewidths of less than 10 MHz. For further details see the chapter by *Sorokina* on mid-IR crystalline lasers and references therein.

1.2 Class "B" Laser Sources

Class "B" laser sources, as defined earlier, are based on parametric frequency conversion of near-IR laser source(s). These can be configured either in resonant (cavity) arrangements with a single pump laser or non-resonant (single-pass) arrangements with two pump lasers and are referred to as optical parametric oscillator (OPO) [46] and difference frequency generation (DFG) based sources, respectively. Figure 3 illustrates these two concepts.

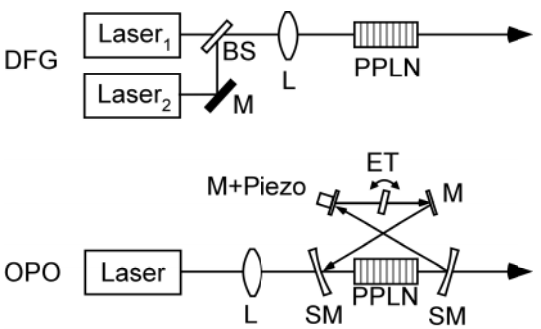

Fig. 3. Shown are two representative examples of DFG and OPO. DFG based mixing uses single pass parametric interaction and requires spatial overlap of the input sources via discrete or optical fiber components. For wavelength tuning, the OPO ring-cavity is wavelength tuned with a piezo driven cavity mirror M. A frequency selector, e.g. étalon, is synchronously tuned to maintain single-mode operation [47]. M, mirror; ET, étalon; L, lens; PPLN, periodically poled lithium niobate; SM, semi-transparent mirror; BS, beamsplitter/combiner

Before discussing the two approaches of parametric frequency conversion, we will discuss a variety of commonly used room-temperature near-IR laser sources that can serve as effective pump sources, followed by a tabulated overview of these sources and their performance characteristics. These laser sources are not emitting mid-IR radiation but can operate at wavelengths ranging from the visible to near-infrared region. However, used in combination with frequency conversion, their spectroscopic characteristics (linewidth, tuning range, etc.) are partially (OPO) or completely transferred to the mid-IR.

1.2.1 Near-IR Pump Laser Sources for Parametric Frequency Conversion

Many of the problems in tuning and wavelength stability of Fabry–Pérot type diode lasers can be enormously reduced by incorporating an external or internal grating structure to provide more defined feedback [48]. In an ECDL (External Cavity Diode Laser) , one or both faces of the laser chip are antireflection-coated to eliminate optical feedback. Instead, the feedback required for laser action is provided by an external cavity. The cavity acts as a narrow wavelength selector, which determines a specific operating wavelength out of the usually broad gain spectrum of the semiconductor laser material. Several cavity configurations have been developed that differ in the method of tuning, number of components, output beam characteristics, and output coupling efficiency. Mode-hop-free single frequency tuning ranges of over 1000 GHz have been demonstrated for an ECDL [49,50,51]. Grating-tuned external cavity diode lasers with large tuning ranges have been commercialized in the near-infrared from 0.9 to 1.6 μm. All ECDL designs have been based on tuning a frequency selector by mechanical means. In environments with technical noise such as vibrations this can lead to additional frequency jitter. More recent designs have incorporated Micro Electro Mechanical Systems (MEMS) technologies, which dramatically reduce the size (5 mm × 5 mm) of the external cavity [52].

Implementation of integrated wavelength mode filters in the form of distributed feedback (DFB) structures or distributed Bragg reflectors (DBR) also enable single frequency operation and have been developed for the optical telecommunication industry at wavelengths ranging from 1.3 to 2 μm. Other novel developments include broadly tunable monolithic integrated multisection diode laser chips employing gain, filter and Bragg tuning elements [53]. Unlike external grating controlled diode lasers, these lasers [54,55,56] offer fast and versatile electronic coarse wavelength tunability ($\approx$ 70 nm at 1.56 μm) of potential pump sources for nonlinear optical frequency conversion devices. Other forms of single frequency near-IR diode laser include VCSEL (Vertical Cavity Surface Emitting Laser), which are simpler and more cost effective to produce, but have not yet reached comparable output powers and IR wavelength coverage. VCSELs can tune over $\approx$ 30 cm^{-1} by changing their operating current (threshold-maximum). Such tuning rates are attractive for

certain applications such as rapid combustion diagnostic studies, but not desirable for precision gas sensing.

Grating stabilized near-IR laser sources have also been developed in the form of rare-earth doped single mode DFB fibers in the 1 μm (Yb) and 1.5 μm (Er) wavelength region. The operating wavelength within the dopant gain region can be precisely engineered to $\approx$ 0.1 nm accuracy by writing a DFB grating via photolithography into a photosensitive doped fiber region. Fiber lasers of this type can be wavelength tuned by means of temperature and straining the DFB fiber length with a piezoelectric element [57]. Ultra-narrow linewidths on the order of a few kHz have been achieved without the use of frequency locking techniques and hence offer convenient high-resolution wavelength tuning capability. In addition DFB fiber lasers offer low relative intensity noise and high side-mode suppression ratios of > 60 dB [`http://www.koheras.com`] [58].

Another important solid-state laser class demonstrated for operation in the near-IR wavelength region is the monolithic non-planar ring oscillator based on Nd, Yb or Tm:YAG materials. This type of laser offers single-frequency CW or pulsed output with diffraction-limited beam quality. Narrow-linewidth CW powers exceeding several watts have been demonstrated [59]. This laser source is specifically suited and used for pumping optical parametric oscillators. For further details see the chapters by Vodopyanov and Ebrahimzadeh.

1.2.2 Sources Based on Difference Frequency Generation (DFG)

Numerous DFG based mid-IR sources have been designed and used for spectroscopy [60,61,62,63,64,65,66,67,68,69,70,71,72]. For further details see also the chapter by Fischer and Sigrist. In the case of DFG, two laser beams ("pump" and "signal") at different frequencies combined in a nonlinear material with suitable dispersion characteristics generate a beam at the difference-frequency ("idler"). The narrow emission spectra of the "pump" (highest frequency) and "signal" (middle frequency) are convolved during the frequency conversion and hence translate into a similarly narrow spectrum of the idler wave. Idler wavelength tuning is accomplished by tuning of the pump laser, or signal laser, or both. In order that the idler wave continue to build up as the beams pass collinearly through the nonlinear material, the three waves must stay in phase (the "phase matching condition"). This imposes a condition on the refractive indices of the three waves.

This condition can often be satisfied with a birefringent nonlinear crystal by having some of the three waves polarized along an ordinary axis and some polarized along a direction that includes the extraordinary axis. If the polarization direction that includes the extraordinary axis is not parallel to it (angle tuning), the three waves will not propagate in the same direction (double refraction) and the beams will separate as they pass through the crystal ("walk-off") limiting the overlap region and the DFG power. In order

Table 5. Summary of tunable near-IR diode, fiber laser and solid-state source characteristics

	Wavelength range (μm)	Tuning (coarse/fine)	Power (mW)	Linewidth	Beam profile characteristics	Operating requirements
ECDL	0.650–1.655	10–100 nm/ 1 cm^{-1} (by Piezo)	1–50	1–5 MHz, 1 s	– Elliptical – Astigmatic – Beam pointing instability with tuning (Littrow design)	Low technical noise environment for best performance. Vibrations lead to increased linewidth of > 100 MHz
SG-DBR-DL	1.55	200 cm^{-1}/ 1 cm^{-1}	2–10	25 MHz, 1 s	– Single mode fiber diffraction limited Gaussian beam quality – Inherent beam pointing stability	– Telecom environment – Requires complex electronics for tuning
DFB-DL	1.3–2	3 nm/ 1 cm^{-1}	2–30	0.1–1 MHz, 1 s	– Single mode fiber diffraction limited Gaussian beam quality – Inherent beam pointing stability	– Telecom environment
DFB Fiber Laser	1.03–1.2 (Yb) 1.528–1.61 (Er)	5 cm^{-1} (Temp.)/ 10 cm^{-1} (PZT)	2–10	0.1 MHz, 1 s	– Single mode fiber diffraction limited Gaussian beam quality – Inherent beam pointing stability	– Telecom environment
Solid-State	0.946, 1.064, 1.319, 1.444, (Nd:YAG) 2.02 (Tm:YAG)	30 GHz (Temp.)/ 100 MHz (piezo)	150–2000 (CW)	0.02 MHz, 1 s	– TEM_{00} ($M^2 < 1.1$)	– Room temperature

ECDL, External Cavity Diode Laser ; SG-DBR-DL, Sampled Grating Distributed Bragg Reflector Diode Laser; DFB, Distributed Feedback Diode Laser

to satisfy phase matching keeping all waves exactly parallel or perpendicular to the optic axis ("90° phase matching"), the refractive indices must be tuned as the difference frequency is tuned by varying the temperature of the crystal or by tuning pump and signal simultaneously.

In the early demonstration of the DFG method by *Pine* [73], single mode argon-ion and dye laser outputs were combined in bulk lithium niobate crystal to produce narrow-band (15 MHz) radiation tunable from 2.2 to 4.2 μm by temperature tuning the crystal. Simultaneous tuning of both signal and pump

has been used in $AgGaS_2$ [64] to provide tunable single frequency radiation from 3.5 to 9 µm. For DFG radiation longer than 5 µm it is also possible to use birefringent bulk nonlinear optical materials, such as $AgGaSe_2$ [74], $ZnGeP_2$ [75], or GaSe [76,77,78].

Another approach to phase matching is the introduction of periodic short (about 10–30 µm wide) regions in which the sign of the second order susceptibility alternates, thus bringing the three waves back into the right phase relationship. This is called quasi-phase-matching (QPM). It is most easily achieved in ferro-electric materials, where the direction of the extraordinary axis can be permanently reversed locally by the application of an external electric field ($\approx$ 20 kV) at elevated temperatures [79]. Other advantages of QPM are no walk-off effects, access to the crystal's largest diagonal nonlinear coefficient (not accessible by birefringent phase-matched crystals), wide acceptance bandwidth, and relative ease of alignment.

The implementation of diode-pumped mid-infrared frequency conversion sources received a significant boost from the development of novel periodically poled nonlinear materials, such as lithium niobate (PPLN) [80], lithium tantalite ($LiTaO_3$), and ferroelectric crystals of the potassium titanyl phosphate ($KTiOPO_4$, or KTP) family at wavelengths in the 2.5–5.2 µm spectral region [81,82,83]. The quasi-phase-matching properties of each of these crystals can be engineered for interaction of any pump and signal wavelengths within the transparency range of the crystal, allowing significant flexibility in the choice of laser sources for frequency mixing [84,85,86]. In the future, quasi-phase matched GaAs [87] should become available greatly extending the long wavelength region covered by DFG. In the work reported by *Eyres* et al. orientation-patterned GaAs films of 200 µm thickness have been grown by hydride vapor phase epitaxy (HVPE) on an orientation-patterned template fabricated by molecular beam epitaxy (MBE).

The availability of PPLN permits near-infrared diode or fiber lasers to be used as pump lasers [68,69,70,71,88,89,90,91,92] instead of much larger dye or Ti:sapphire lasers making it feasible to construct compact mid-infrared spectrometers that operate at room temperature and can generate CW output powers up to 1 mW [93]. Thus the practicality of near-infrared diode laser and optical fiber technology are combined to achieve the analytical power of mid-infrared spectroscopy in a single instrument. Such an instrument inherits the single-frequency operation and high modulation speed capabilities of diode lasers, and takes advantage of their relatively wide tuning range. For example, a typical 780-nm diode laser can be grating tuned over 20 nm, or 2.6 % in wavelength without appreciable changes in output power. When the output of such a laser is down-converted by mixing with a 980 nm diode laser, the tuning range in frequency units remains the same, in this case a significant tuning range: 3.6–4.1 µm, or 13 % in wavelength.

A detailed quantitative theory of this nonlinear optical process is beyond the scope of this review chapter. Instead, the reader is referred to a paper by

Zondy [94] and the references contained therein. Therefore, we will simply state that the maximum idler power generated in a given crystal is proportional to the product of crystal length, pump power, signal power, and the square of the second-order nonlinear coefficient of the crystal. Optimum DFG output power is achieved by means of precise spatial overlap and focusing of the pump and signal beams. There is an optimal focus because a point is reached at which any further increase in beam intensity through tighter focusing is offset by a decrease in interaction length due to diffraction, resulting in loss of output power and in some cases clipping at the crystal aperture. Although this type of source is routinely used for spectroscopy and gas detection, DFG in bulk nonlinear (either birefringent or quasi-phase matched) crystals is characterized by low conversion efficiency, typically [95] in the range 0.002–0.05 % $W^{-1}\,cm^{-1}$.

The tradeoff between beam size and interaction length can be eliminated in guided-wave DFG. Optical confinement of pump and signal radiation near the waveguide core creates a region of high intensity and good modal overlap that can be maintained throughout the length of the waveguide. Thus the interaction length for tight focusing is now limited by the length of the waveguide, not by diffraction. Guided-wave parametric processes, such as OPO, SHG, and DFG, have been demonstrated [96] in periodically poled $LiNbO_3$, $LiTaO_3$, and KTP. In $LiNbO_3$, for example, a waveguide can be formed by titanium in-diffusion, or by a Li^+–H^+ ion exchange typically followed by several hours of annealing at elevated temperature to create a graded index distribution.

A DFG waveguide designed to carry a single spatial mode at the idler wavelength is necessarily multimode at the shorter, pump and signal wavelengths. The presence of multiple spatial modes complicates waveguide phase matching characteristics. For example, a TEM_{00} (fundamental) mode at the signal wavelength will interact with TEM_{02} and TEM_{10} modes at the pump wavelength, but not with TEM_{01} or TEM_{11} modes. Efficient and reproducible fundamental-mode excitation of a DFG waveguide was first achieved by *Chou* et al. [96,97] using a combination of a mode filter and an adiabatic taper. An improved device featuring separate inputs for the pump and signal beams followed by a directional coupler has also been demonstrated. DFG waveguides have been used to build sources of mid-infrared radiation for spectroscopic purposes [98,99,100]. Surprisingly, though, reported idler power from waveguide-DFG have not exceeded powers of more than 0.1 mW, whereas with bulk QPM DFG crystals, powers exceeding 1 mW have been obtained through use of high input power sources. Difficulties in efficiently coupling the pump laser power into the waveguide and maintaining the waveguide properties in the presence of higher power fields have so far prevented the generation of higher mid-IR power levels that exceed those obtained with bulk QPM DFG crystals. In addition, waveguide-QPM structures have relatively narrow conversion bandwidths, whereas bulk-QPM can be poled to

have either multiple grating periods or a fan-out structure for continuous phasematching over 750 cm^{-1} [69].

Table 6. Summary of difference frequency generation based sources

Wavelength range (μm)	Tuning (coarse/fine)	Power (mW)	Linewidth	Beam profile characteristics	Operating requirements
2.3–4.6 (based on available near-IR telecom laser wavelengths)	15 cm^{-1} per diode laser pair; wavelength multiplexing possible/ 2 cm^{-1}	0.1–1 mW	1 MHz	– Near Gaussian (fiber pump beam delivery only) – Beam pointing stability – large f/# ≈ 100	Telecom environment

1.2.3 Tunable Optical Parametric Oscillators

Optical parametric oscillators (OPOs) are progressing as useful spectroscopic tools for the generation of coherent radiation that is continuously tunable over large spectral ranges [101,102,103,104,105,106,107]. For further details see the chapters by Vodopyanov and Ebrahimzadeh. Unlike DFG, the nonlinear crystal is placed in a cavity and is used to generate output beams at two new frequencies (signal and idler) ν_1 and ν_2 from a single pump beam at ν_3 (Fig. 3). Energy conservation requires $\nu_1 + \nu_2 = \nu_3$. How the frequency is divided between the new waves, signal and idler is determined by the phase-matching condition. The development of pulsed OPOs is mature, and these devices are available commercially. On the other hand, CW OPOs still have some practical problems in terms of requiring high power pump sources, efficient and high quality nonlinear crystals, low loss broadband optics, and mode-hop-free operation with good frequency stability in order to realize their potential usefulness in mid-IR spectroscopic power.

OPO devices are arranged so that the signal frequency resonates inside the cavity (singly resonant OPO), or in addition the idler can also be made resonant (doubly resonant OPO). In some special cases the pump frequency can be made resonant as well (triply resonant OPO). In principle, both doubly resonant and singly resonant OPO configurations can be used although as a practical matter doubly resonant OPOs are difficult to construct and cumbersome to tune.

As in DFG devices quasi-phase-matching in periodically poled ferroelectric crystals offers several distinct advantages for their use in CW OPOs, such as non-critical phase matching and a high effective nonlinear coefficient, d_{eff}. A particularly significant development was the demonstration of the use of PPLN as the parametric gain medium, in which case the oscillation threshold of externally pumped CW singly resonant OPOs can be reduced to the few watt level hence making it feasible to use diode pumped solid-state pump

lasers [101,102,103,104,105,106,108,109,110,111,112,113,114]. Pump powers as low as 800 mW were used to pump a PPLN singly resonant OPO in which both the pump and signal were resonated [115].

The parametric process can also be used in optical parametric amplifiers (OPAs) to boost infrared output powers. Continuous wave OPOs amplified by pulsed OPAs offer a competitive alternative to other tunable lasers in the 1–5 μm spectral region in terms of linewidths, wavelength tunability and output powers.

Table 7. Summary of OPO (PPLN based) characteristics [116]

Wavelength range (μm)	Tuning (coarse/fine)	Power (mW)	Linewidth	Beam profile characteristics	Operating requirements
1.45–2 2.3–4	$1900\,\mathrm{cm}^{-1}$/ $0.05\,\mathrm{cm}^{-1}$	10– 100 mW	0.15 MHz, instantaneous	TEM_{00}	Low technical noise environment

2 Fundamentals of Absorption Spectroscopy for Trace Gas Detection

Spectroscopic trace gas detection is a method allowing one to determine the concentration of a *known* gas, or gases, from a measured optical absorption spectrum of the gas mixture (in practice, a small fragment of the spectrum is measured). The procedure requires a good quantitative knowledge of the gas absorption characteristics. This knowledge is the realm of molecular spectroscopy, a complex and highly developed subject. A few fundamental spectroscopic concepts and formulae that are directly applicable to gas detection are, however, summarized in this section.

Each atom or molecule, small or large, is uniquely characterized by a set of energy levels. Transitions between levels by absorption or emission of electromagnetic radiation result in highly specific spectroscopic features. These features allow both the identification and quantification of the molecular species, such as atmospheric trace gases. Molecules may undergo transitions between electronic, vibrational, and rotational states when exposed to electromagnetic radiation, resulting in absorption spectra. These spectra consist of a number of discrete absorption *lines*. Each line will have a certain linewidth and shape that depends on temperature and what surrounds the molecule. The lines may in some cases be resolved and in other cases the line density may be too high to be spectrally resolved. Transitions between molecular rotational-vibrational ("ro-vibrational") states occur in the infrared "fingerprint" region of the electromagnetic spectrum, approximately between the wavelengths of 2.5 and 25 μm. Also, overtone and combination-overtone ro-vibrational lines are possible with significantly lower intensities as compared to those for fundamental vibrational bands and the corresponding wavelengths are in the

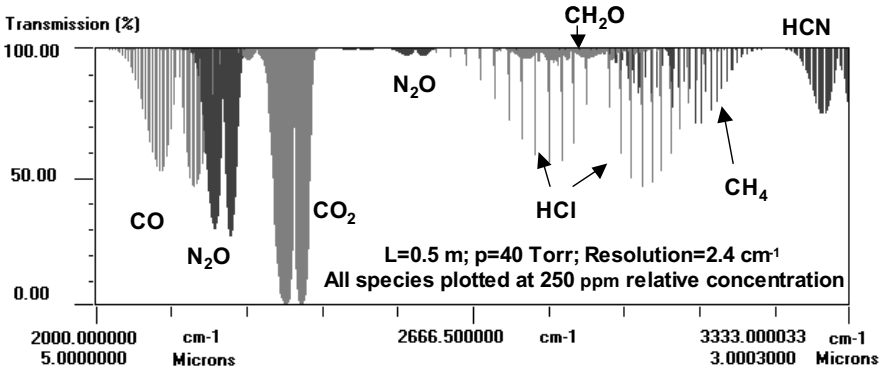

Fig. 4. HITRAN simulation of absorption bands of various molecules in the 3–5 μm spectral region. All species are plotted with identical relative concentration. Spectral overlap limits the choices of interference free absorption lines

0.8–2.5 μm spectral region. Transitions between electronic states of atoms and molecules occur in the ultraviolet and visible spectral region.

All polyatomic molecules, with the exception of homonuclear diatomic molecules (e.g. N_2), absorb infrared radiation. The absorption changes the state of molecular rotation and vibration. An absorption spectrum therefore depends on the physical properties of the molecule such as size and shape and hence each molecule is characterized by a unique spectral "signature". Spectra of linear and some nonlinear polyatomic molecules consist of an array of individual or small groups of lines. In the case of large polyatomic molecules (e.g. benzene, C_6H_6) at atmospheric pressure, there are many lines overlapping each other, resulting in broad spectral features with some occasional peaks.

There are numerous atmospheric trace gases and their concentrations are normally in the parts-per-trillion (pptv, 10^{-12}), parts-per-billion (ppbv, 10^{-9}) to parts-per-million (ppmv, 10^{-6}) range. However, species such as water vapor may have concentrations of up to a few percent (%, 10^{-2}). Because of this, even weak water features, where absorption cross-sections are as much as a factor of 10^{-10} weaker than the molecule of interest, can be a problem.

There is much spectroscopic data available in the literature and in electronic form which are important tools in the identification and development of specific detection strategies, especially in the presence of interfering species [117,118].

Direct gas phase laser absorption spectroscopy based on the Beer–Lambert absorption law is often used for quantitative measurements.

In the absence of optical saturation and particulate-related scattering, the intensity of light $I(x)$ propagating in a homogeneous gas of sample length L

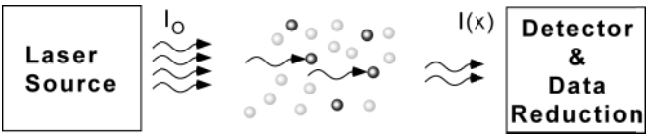

Fig. 5. Illustration of the Beer–Lambert absorption law

follows the Beer–Lambert law:

$$I(x) = I_0 \exp\left[-\sigma(\nu) N L\right] . \tag{1}$$

Here N represents the molecular concentration and $\sigma(\nu)$ the absorption cross-section. The molecular absorption cross-section depends on frequency and has units of $\mathrm{cm}^2\ \mathrm{cm}^{-1}$ per molecule when integrated over the absorption line, and units of cm^2 per molecule at the line center. For simplicity we assume only one absorbing species. The peak absorption cross-section at line center (ν_0) is related to the integrated line strength through a lineshape function $\Gamma(\nu)$. This function $\Gamma(\nu)$ has the same analytical form for all transitions, and in mid-infrared spectroscopy, the broadening of an individual transition due to finite upper-level lifetime is insignificant compared to broadening by the other two important mechanisms – thermal motion and molecular collisions. Their individual and combined effects on a molecular transition at a frequency ν_n are expressed as follows:

Thermal motion (Gaussian):

$$\Gamma_\mathrm{D}(\nu) = \frac{1}{\gamma_\mathrm{D}} \sqrt{\frac{\ln 2}{\pi}} \mathrm{e}^{-\left(\frac{\nu-\nu_0}{\gamma_\mathrm{D}}\right)^2 \ln 2} ; \quad \gamma_\mathrm{D} = 3.58 \times 10^{-7} \nu_0 \sqrt{\frac{T}{M}} , \tag{2}$$

Molecular collisions (Lorentzian):

$$\Gamma_\mathrm{L}(\nu) = \frac{1}{\pi} \frac{\gamma_\mathrm{L}}{(\nu_0 - \nu)^2 + \gamma_\mathrm{L}^2} ; \quad \gamma_\mathrm{L} = \gamma_\mathrm{L}^0 p \sqrt{\frac{T}{T_0}} , \tag{3}$$

Combined broadening (Voigt):

$$\Gamma(\nu) = k(\nu_0)_\mathrm{D} \frac{y}{\pi} \int_{-\infty}^{\infty} \frac{\mathrm{e}^{-t^2}}{y^2 + (x-t)^2} \mathrm{d}t ; \quad k(\nu_0)_\mathrm{D} = \frac{\int \sigma(\nu) \mathrm{d}\nu}{\gamma_\mathrm{D}} \sqrt{\frac{\ln 2}{\pi}} , \tag{4}$$

with,

$$x = \left(\frac{\nu - \nu_0}{\gamma_\mathrm{D}}\right) \sqrt{\ln 2} ; y = \frac{\gamma_\mathrm{L}}{\gamma_\mathrm{D}} \sqrt{\ln 2} ; t = \left(\frac{\delta}{\gamma_\mathrm{D}}\right) \sqrt{\ln 2} .$$

Here T is the gas temperature (K), M the molecular weight, P the gas pressure (atm), and γ_L^0 the coefficient of pressure broadening ($\mathrm{cm}^{-1}\mathrm{atm}^{-1}$), $k(\nu_0)_\mathrm{D}$ is the peak Doppler cross-section, δ is the parameter of integration

and is used to express the Doppler and Lorentz frequency differences during the convolution process in terms of a single variable. The quantities γ_D and γ_L are referred to as the Doppler- and pressure-broadened half width at half maximum (HWHM) linewidths. The line shape that results from the combined effect of Doppler- and pressure-broadening is a convolution of the two respective line shapes, and it is known as the Voigt profile. The physical significance of the convolution is that the Voigt profile has different asymptotic shapes for very low and very high gas pressure. At low pressure, molecular collisions are less frequent, leaving thermal motion the dominant broadening mechanism – the corresponding line shape is near-Gaussian. As the gas pressure increases the collisions take over, and the resulting line shape is near-Lorentzian (Fig. 6).

The previous expressions do not include the effect of pressure shift, which is typically in the range of several megahertz per atmosphere. The shift is very small compared to the width of an atmospheric-pressure-broadened line, typically several gigahertz. It can be verified by integrating the absorption cross-section of an individual transition over frequency, that the shift is *independent* of the broadening mechanism and is equal to the line intensity S, in units of $\mathrm{cm}^2\,\mathrm{cm}^{-1}$ per molecule. The line intensity is proportional to the lower-state population density of a transition and thus depends on temperature. These parameters have been measured and calculated for many lightweight gas molecules in the mid-infrared

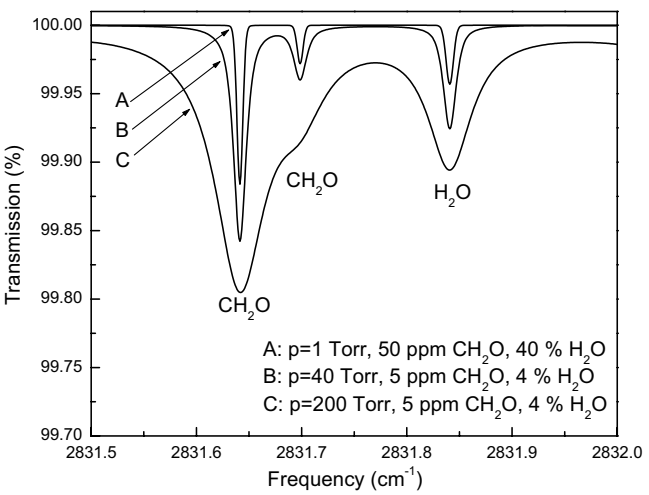

Fig. 6. Computed mid-IR absorption spectra of CH_2O and H_2O at 1, 40 and 200 Torr. Lineshapes correspond to near-Gaussian (A), Voigt (B) and near-Lorentzian (C). Also note the higher relative concentration at lower pressures to obtain a comparable absorption strength. Optimum sampling pressure with good signal strength and selectivity ranges typically between 30 and 60 Torr

spectrum, and compiled into extensive databases such as HITRAN [117], GEISA [118], NIST (`http://ois.nist.gov/srmcatalog/datafiles`), and PNNL (`http://nwir.pnl.gov`). Numerically accurate absorption spectra can be computed based on these data, not only for single gas species but for gas mixtures as well.

The analytical formulae apply also to multi-component gas mixtures. The total absorption cross-section $\sigma(\nu)$ is then a weighted average of absorption cross-sections of individual species, with the mole fraction C_{m} of each species used as the weight coefficient:

$$\sigma(\nu) = \sum_{\mathrm{m}} C_{\mathrm{m}} \sigma_{\mathrm{m}}(\nu)\,, \quad \sum_{\mathrm{m}} C : \mathrm{m} = 1\,. \tag{5}$$

For each of the m species, the pressure broadening coefficients γ_{L}^{0} generally depend on the transition. They also depend on the type of molecule with which the collisions occur. In general, partial pressures in conjunction with the appropriate pressure-broadening coefficients should be used to compute the overall pressure broadening from all gases present in the background (this includes self-broadening). Air-broadening coefficients are useful in calculations, and are listed in spectroscopic databases [117,118].

In trace gas sensing applications, however, the species of interest are often present in very low concentrations, so that self-broadening and broadening against other trace gases can be neglected in calculations, and air-broadening alone will suffice. For the conditions of atmospheric pressure broadening, $\gamma_{\mathrm{L}}^{0} P \gg \gamma_{\mathrm{D}}$, the Doppler contribution to the overall linewidth can often be neglected, and the line shape be treated as pure Lorentzian. Likewise, at pressures low enough to ensure $\gamma_{\mathrm{L}}^{0} P \ll \gamma_{\mathrm{D}}$, the line shape can be treated as pure Gaussian. In either case, calculation of the line profile is simplified considerably.

At intermediate total pressures, $\gamma_{\mathrm{L}}^{0} P \approx \gamma_{\mathrm{D}}$, which for most lightweight gases range from 5 to 100 Torr, calculation of the Voigt profile is necessary to obtain numerically accurate absorption spectra. Methods for approximate calculation of the Voigt profile, and the related plasma dispersion function, are now a well-developed subject. The approximations published in [119] are particularly useful.

3 Spectroscopic Techniques: Signal Enhancement and Noise Reduction

In direct absorption approaches, quantitative information can be obtained using the expressions discussed in the previous section.

This section only discusses *in situ* techniques, where the source, sampling region and the detector are in close proximity. Active remote sensing such as differential optical absorption spectroscopy (DOAS) and light detection and ranging (LIDAR) are well developed, but not covered here and the interested

reader is referred to the following recent book chapters by *Platt* [120] and by *Svanberg* [121].

For *in situ* measurements, various sensitivity enhancement and noise reduction spectroscopic detection techniques have been developed in order to achieve quantification of trace gas species at concentrations ranging from ppmv to pptv. Each detection technique has its distinct advantages and should be chosen depending on the specific application targeted, in particular in terms of sensitivity and selectivity requirements.

Although laser source noise is an important aspect for sensitive detection, in practice various other noise sources affect the measurement of a small change of signal and can severely limit the detection sensitivity. Various noise reduction techniques can be employed. These include modulation, balanced beam and zero-background subtraction detection techniques. In addition, one can improve the sensitivity by signal enhancement methods based on long pathlength and cavity enhanced spectroscopy (Sects. 3.3 and 3.4), which are capable of increasing significantly the effective sample optical pathlength L to tens of meters and to kilometers, respectively, in absorption cells of typical physical lengths of 0.3 to 1 m.

It is difficult to compare the expressions of sensitivity in terms of trace gas detection systems that employ different sources and detection techniques and their significance for a specific application. In this context, different expressions of sensitivities reported in the literature are a relative statement and can be at times misleading if applied or compared to a different signal enhancement or noise reduction technique. Perhaps the most appropriate method to compare the performance of trace gas detection systems (laser and even non-laser based) is to determine the minimum detectable concentration for the target molecule of interest for a given sampling and acquisition time. For comparisons with other techniques one can relate this to a minimum detectable absorbance per pathlength for the pathlength conditions employed in the concentration measurement. We make this distinction since, for example, in photoacoustic spectroscopy one obtains very high sensitivity for unit pathlength, however it does not directly scale with increasing pathlength. In many cases, such as isotopic ratio measurements, the replication precision is most important. These and other attributes such as wavelength dependent absorption strengths should be given detailed consideration before selecting a laser source and technique for a specific trace gas sensor. Table 8 gives an overview of the most commonly used expressions and depicts examples of values achieved and reported in the literature.

3.1 Balanced Beam and Balanced Ratiometric Detection (Noise Reduction)

These techniques have been developed in order to eliminate technical noise including laser intensity noise to approach the fundamental limit of shot-noise. By measuring the laser signal with and without the absorption signal

Table 8. Expressions of detection limits and sensitivity

Parameter	Expression	Common values/units
Minimum detectable fractional absorption	$\frac{\Delta P_{\min}}{P_0}$	10^{-4}–10^{-7}
Minimum detectable fractional absorption scaled to path length	$\frac{\Delta P_{\min}}{P_0}\frac{1}{L}$	10^{-8}–$10^{-12}\,\mathrm{cm}^{-1}$
Minimum relative Detectable Concentration per unit volume (MDC)	$\frac{\Delta P_{\min}}{P_0}\frac{1}{L}\frac{1}{\sigma N_{\mathrm{tot}}}$	ppm (1 part in 1 million) 10^{-6} ppb (1 part in 1 billion) 10^{-9} ppt (1 part in 1 trillion) 10^{-12}
Minimum detectable fractional absorption scaled to path length, relative concentration, and per shot measurement time	$\frac{\Delta P_{\min}}{P_0}\frac{1}{L}\frac{1}{\sigma N_{\mathrm{tot}}}\frac{1}{\sqrt{\mathrm{BW}}}$	10^{-8}–$10^{-12}\,\mathrm{cm}^{-1}\,\mathrm{Hz}^{-1/2}$ $\mathrm{BW} = \frac{\#\mathrm{pts}}{T_{\mathrm{sample}}n}$ or $\frac{\mathrm{ENBW}}{n}$ Bandwidth(BW) without or with a frequency selective filter (e.g. lock-in amplifier)
Absolute Laser Instrument Response Factor (LIRF)	$\frac{\Delta P_{\min}}{P_0}\frac{1}{L}$ with $T_{\mathrm{meas,total}}$	$10^{-8}\,\mathrm{cm}^{-1}(1\,\mathrm{s})$–$10^{-11}\,\mathrm{cm}^{-1}(60\,\mathrm{s})$
Measurement precision (measured with a stable input concentration)	Std.Dev. (LIRF) or Std.Dev. (MDC)	

Legend in order of appearance

P, optical power; L, length of effective light–matter interaction; σ, molecular absorption cross-section [cm^2]; N_{tot}, total number of molecules per unit volume; #pts, number of acquired points per scan; T_{sample}, time for single scan; n, number of acquired scans; ENBW, equivalent noise bandwidth of a frequency selective filter; $T_{\mathrm{meas,total}}$, measurement time to generate one concentration data point

simultaneously, common mode noise can be subtracted and small absorption signals can be recovered. Several approaches using dual-beam detection have appeared in the literature and are briefly discussed here.

Conventional dual-beam detection systems use optical balancing schemes [122]. The detected noise of an equal-intensity replica of a probe beam, such as that created by a variable-ratio beamsplitter, is subtracted from noise detected in the probe beam and thus leaving only the uncompensated weak absorption signals of interest. For example, such a beamsplitter can be realized by placing a polarization rotator (a half-wave plate) in series with a polarizing beamsplitter cube. With the input polarization ro-

tated about 45°, the beams emerging from the beamsplitter cube carry equal amounts of power P, and power noise ΔP. In the absence of absorption, the photocurrents generated by identical signal and reference detectors can be subtracted to cancel each other exactly. If one of the beams is attenuated due to small absorption a, by a gas, the balance of photocurrents is disturbed, and a signal is seen at the output of the amplifier. Care must be exercised to ensure that the signal and reference detectors have equal amplitude and frequency responses.

An implementation of this method that avoids the need for exact balancing the signal and reference light was proposed by *Hobbs* [123]. It is known as balanced ratiometric detection (BRD). It employs electronic circuitry to produce a log ratio of photocurrents, rather than their difference, *and* to cancel noise currents at the same time. This analog divider uses logarithmic conformance and tight symmetry of base-emitter curves of a matched transistor pair. This scheme provides nearly perfect cancellation of noise currents even when the reference beam carries twice the power of the signal beam. Since the signal versus reference current balancing is performed by means of electronic feedback, no physical adjustment of the beam splitting ratio is necessary. The BRD differential response to absorption signals depends on the ratio of the signal and reference currents, which changes when the signal beam is partially absorbed. It also depends on temperature because the transistor base-emitter voltage does, and additional compensation circuitry is needed to produce a useful output voltage V_{out} that is linearly proportional to the absorbance. Noise-equivalent absorbances in the near-infrared spectral region as low as $2 \times 10^{-7}\,\text{Hz}^{-1/2}$ have been demonstrated by *Allen* and co-workers [124], close to the limit imposed by shot noise. Application of this concept to the mid-IR spectral region using a quasi-CW QC laser was recently demonstrated by *Sonnenfroh* et al. [125] However, the sensitivity was reduced due to inherent differences of the employed mid-IR detectors with large background currents derived from each detector and low average photocurrents. Improvements to the design may well translate the results obtained in the near-IR and yield sensitivities of $\approx 1 \times 10^{-5}$.

Ratiometric detectors have been shown to greatly reduce technical noise and enhance the sensitivity with short path distances. Technical noise originating from optical elements that are only present in either sample or reference beam are not cancelled. This limits the use of a BRD to noise reduction with common optical paths. For example, technical noise from multi-pass optical cells cannot be eliminated by this technique and hence extrapolation of short-path sensitivities does not scale with longer pathlengths. BRD is therefore well suited for low-noise measurement application using compact short-path absorption cells.

3.2 Wavelength and Frequency-Modulation Spectroscopy (Noise Reduction)

As discussed in Sect. 1.1, the output wavelength of diode lasers can be changed by either changing the entire device temperature or by changing the injection current. The latter tuning mechanism is very rapid, thus making it possible to employ high frequency modulation techniques in the kHz to MHz regime. Traditionally, these two frequencies are used to describe two different modulation approaches. Modulation employing frequencies in the kHz regime is denoted as wavelength modulation spectroscopy (WMS). This approach, which is also known as harmonic detection or derivative spectroscopy, uses a modulation frequency ($\approx$ 1–100 kHz) that is much less than the half width of the laser source employed, which typically ranges between several MHz to hundreds of MHz. By contrast, frequency modulation spectroscopy (FMS) is characterized by modulation frequencies greater than the laser line half width and typically involves frequencies up to several hundred MHz.

Frequency modulation is always accompanied by amplitude modulation, as the injection current also controls the laser output power:

$$E(t) = A[1 + m\cos(\Omega t)]\sin[\omega t + \beta\cos(\Omega t + \Phi)]\,. \tag{6}$$

Here $E(t)$ is the laser electric field, $\omega = 2\pi c/\lambda$ the laser frequency, and Ω the modulation frequency. The quantities m and β are the amplitude and frequency modulation indices, respectively, and Φ is the generally non-zero phase shift. Sine-wave modulation of the diode laser has the effect of creating multiple side-bands in its otherwise nearly monochromatic emission spectrum. Each side-band is separated from the carrier by an integer multiple of the modulation frequency Ω, and its relative intensity depends on β.

In frequency-modulation spectroscopy, Ω significantly exceeds the laser linewidth that is typically several tens of megahertz, and m, β are both small, so that only the two first-order side-bands, $\omega + \Omega$ and $\omega - \Omega$, have appreciable magnitude. After uniform attenuation, such as that encountered in non-resonant optical systems or media, the side-bands add up coherently with the carrier and balance each other to produce a beam of nearly constant intensity, A^2. If the attenuation strongly depends on frequency, however, as is the case with most gases, one of the side-bands may become unbalanced and lead to the appearance of multiple harmonics of Ω in the detected laser intensity. The strength of absorption determines the magnitude of these harmonics, which may be measured separately and with high noise immunity, by using a lock-in amplifier for example. This is usually done while the laser carrier frequency ω is scanned in the vicinity of the absorption line of interest.

This detection technique was first applied by *Bjorklund* to a CW dye laser [126]. It has proved very effective and is used in diode laser spectroscopy today, sometimes in modified form such as two-tone frequency-modulation (TTFM) [127], or amplitude-modulated phase-modulation (AMPM) spectroscopy [128].

In WMS, which is really another form of FM spectroscopy, the modulation frequency Ω is smaller than the laser linewidth, and the modulation indices m and β are both large [129,130,131]. The side-bands are then present to a very high order and due to their small separation from each other, merge into a continuous spectrum. The detection is again performed at the first, second, or higher harmonics of Ω as the laser carrier frequency ω is scanned in the vicinity of a gas absorption line. Lock-in amplifiers or mixers are employed in this approach in selecting the harmonic of choice, which in most cases is the second harmonic. WMS is used in applications that rely on relatively low-speed detectors, and its inherent sensitivity is typically limited by the laser amplitude $1/f$ noise [132]. However, optical noise often limits the sensitivity achievable using both WMS and FMS techniques in real world systems. In addition, as discussed by *Werle* [133], an FM spectrometer can be interpreted as an optimized single beam interferometer. In this model, as the modulation frequency is increased the measurements become more sensitive to small changes in the optical path, thus ultimately resulting in less stability relative to WMS techniques. Both of these issues may explain the fact that the expected improvements with FMS over WMS have not been realized on a routine basis.

As an alternative to modulation spectroscopy, some research groups have been very successful in achieving noise reduction by sweeping the laser injection current at kHz rates and detecting the resulting direct absorption spectrum using a signal averager (see for example, *Zahniser* et al. [134]). When coupled with background subtraction (to be discussed in Sect. 4.1.1) absorption sensitivities in the 10^{-6} range have been achieved. This approach has the advantage over modulation techniques in providing a direct measure of the sample concentration using the Beer–Lambert absorption law without the need for calibration standards and lock-in amplifiers or mixers, required for modulation approaches. In addition, as all modulation techniques effectively smear the peak absorbance at the line center with absorbance in the wings, the effective line center absorbance is reduced. *Fried* et al. [135], *Iguchi* [136] and references therein indicate that the effective line center absorbance using modulation approaches is only 30–50 % of that achieved employing direct absorption approaches. The exact reduction depends upon the particular modulation function employed. On the other hand, modulation spectroscopy presents some advantages over rapid sweep integration direct absorption spectroscopy. In modulation spectroscopy one has some flexibility to choose the modulation amplitude and frequency to minimize dominant optical noise features that may be present in direct absorption techniques. Furthermore, since modulation techniques rely on a "fast" change in the absorption coefficient with wavelength, these approaches discriminate against broad featureless absorptions, such as those from the wings of atmospheric pressure water lines and those from big unresolved organic molecules. This aspect, which is often overlooked, becomes important as an added degree of selectivity when

measuring trace gas concentrations in the atmosphere at levels of 100 pptv or less. Even though one may select an isolated absorption line to quantify a particular gas of interest using the HITRAN database [117], there exists the possibility that numerous broad featureless organic molecules, that can be present in the atmosphere, may spectrally overlap the absorption line of interest. In such cases, direct absorption measurements may yield systematic errors.

3.3 Long Optical Path Length Spectroscopy (Signal Enhancement)

One of the most obvious ways to enhance the absorption signal is inherent to the Beer–Lambert absorption law, where the linear signal improves with longer optical pathlengths. Traditionally, this has been implemented by the use of optical multi-pass cells. Four types of multi-pass cells are most commonly applied: *White* cells [137,138], *Herriott* cells [139], *Chernin* [140] and astigmatic mirror multi-pass cells [141]. For all four types of cells, the focusing mirror curvature, applied to the beam at each reflection, keeps the beam from diverging. The *White* cell [137,138] is the oldest arrangement. It consisits of two semicircular mirrors, called the "D" mirrors, closely spaced along a common diameter facing a third notched mirror in a nearly confocal arrangement. The probe beam enters through one notch and emerges through the other. The number of passes is varied by changing the "D" mirror angle. The *Herriott* cell [139] has two identical spherical mirrors separated by nearly their diameter of curvature (nearly concentric) facing each other. A probe beam launched through a hole in one of the mirrors at an angle to the optical axis, completes a certain number of passes between the mirrors, and exits through the same hole (or a hole in the other mirror). The beam bounce pattern and pathlength are controlled by adjusting the mirror separation. For both the White and the Herriott configurations, the number of passes, if not limited by attenuation of light due to the finite mirror reflectivity, is limited by the overlapping of spots on the mirrors. Spot overlapping creates optical interferences causing base line oscillations superimposed on the absorption feature. Astigmatic mirror cells [141] are variations of the Herriott cell that spread the light spots over the entire mirror surfaces. This greatly increases the number of spots achievable without overlapping spots and therefore the number of passes. This cell type is also more compact and possesses the smallest cell volume to effective path length ratio. In such a multi-pass cell, the number of passes is typically configured for 90–238, which translates to effective optical pathlengths from 18 m to 210 m for mirror separations of 0.3 m–0.9 m, thus providing a commensurate improvement in signal strength. The cell volume of multi-pass cells scales with the number of passes and mirror separation. Respective volumes for the aforementioned astigmatic cells range from 0.3–5.2 l. Hence, longer optical pathlengths also increase the surface area and flushing

time and ultimately determine the speed of measurement. The four multi-pass arrangements are commonly enclosed in a vacuum housing, and used for the measurement of static gas samples or controlled gas flows, but can also be operated without enclosure for open-path ambient air trace gas monitoring applications.

Multi-pass-cell mirrors can be configured for broadband laser wavelength operation (from the near IR to the long-mid-IR region by use of gold or silver coated mirrors) or can be optimized for specific wavelength regions by using dielectrically coated mirrors similar to mirrors used in cavity ring down spectroscopy. Metallically coated mirrors have a typical reflectivity of $> 99\,\%$, resulting in a cell transmission of $16\,\%$ for 182 passes. Cell transmissions can be greatly enhanced by the use of dielectrically coated mirrors, but at the expense of a narrower wavelength operation. The beam entrance and output coupling holes are a few mm in diameter. To avoid extensive beam aperture clipping resulting in forward and backscattering, the entering beam must be matched to the f/# of the multi-pass cell. Furthermore, the beam spots on the mirror are separated by a finite width. Thus, the higher the f/# and the smaller the beam size, the less optical interference may occur. The beam pointing stability is another important factor as it can have a multiplicative effect on the effective pathlength and hence produce jitter in the absorption signal. Slow minute changes of the beam direction may also superimpose baseline fluctuations. By flushing the multi-pass cell with "zero-air" and acquiring the background, this effect can be captured and removed. To obtain a high measurement duty cycle, the beam pointing instability must be minimized and the multi-pass cell be mounted on a rugged platform.

3.4 Cavity-Enhanced Spectroscopy Methods (Signal Enhancement)

Another technique, which takes advantage of long optical path length absorption in high finesse optical cavities, is called cavity-enhanced spectroscopy. Various methods have been developed. Cavity ring-down spectroscopy (CRDS), first demonstrated by *O'Keefe* and *Deacon* [142], is based on the observation of the decay rate of an injected laser beam stored in a cavity comprised of ultra-high reflective spherical mirrors. The rate of decay (inverse of the ring-down time constant) is determined by a) mirror absorption and scattering, and b) wavelength dependent absorption loss by the inserted sample gas. If the decay rate of a) is determined in the presence of a non-absorbing gas or at a non-gas absorbing wavelength, then the gas concentration is exactly proportional to the difference of the observed inverse sample decay rates. Figure 7 illustrates the concept of CRDS. Also shown is the inherent difference to direct absorption spectroscopy. The decay rate is independent of laser amplitude, which relaxes the requirements of the laser source, in particular for pulsed sources with high pulse-to-pulse variations.

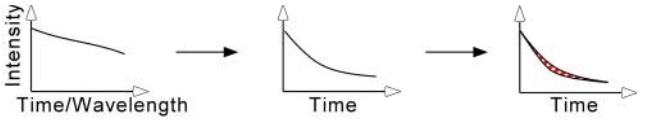

Fig. 7. Concept of CRDS. Shown are the laser signal as a function of time and wavelength before an absorption cell, and the time evolving signal at the detector, after the laser radiation has stopped or is blocked from entering an absorption cell, with and without a sample present. The difference of the decay rate of the sample and 'empty' cell is recorded. The integrated area or difference of the inverse decay rates is directly proportional to the gas concentration

Due to the large effective pathlengths (1 to 10 km is typical, 100 km has been demonstrated), this technique offers significantly higher signal enhancement than is obtainable in conventional absorption spectroscopy. A typical CRDS cell has a base pathlength ranging from 0.5 m to 1 m. The mirrors in such a cell can be designed for specific wavelength regions from the ultraviolet ($\approx$ 300 nm) to the mid-IR spectral region (10 µm). High reflectivity coatings of 99.95–99.99 % in the mid-infrared are commercially available. Although these are very small differences in the mirror reflectivity, the resulting effective pathlength can be significant. For example, a 0.5 m cavity equipped with identical 99.98 % reflectivity mirrors yields a pathlength of $\approx$ 2500 m, whereas with 99.99 % reflectivity, an effective pathlength of 5000 m may be obtained. These pathlengths give ring-down times exceeding 10 µs. If the minimum detectable fractional absorption determined by the decay rates is constant, this results in a 50 % change of minimum detectable concentration. The high reflectivity is usually retained over $\approx$ 10 % of the center wavelength, thus over a typical absorption scan no changes of pathlength need to be considered and even multiple species detection can be implemented with a single set of mirrors. Tests with a variety of gases indicate stability of the mirror reflectivity without noticeable degradation [143]. Condensation on mirrors can be avoided by heating the mirrors to 70 °C or higher without damage [144]. Nevertheless, one should avoid deposits of any kind on the mirrors, and one method successfully used is to employ a clean air purge flow over the mirrors. A second practical consideration relating to the very high mirror reflectivity deals with the amount of light that can be injected into the cavity and the amount that can be extracted and detected. For CRDS, the output intensity can be on the order of 10 % of the input intensity. For non-resonant cavity enhanced spectroscopy methods, the transmitted intensity is on the order of the transmission through a single mirror.

In the following two sections, we provide an overview of the inherent merits of this absorption measurement technique in the mid-IR wavelength region. We describe technical challenges and solutions of several approaches. We will also give examples on how this technique compares to established spectro-

scopic techniques. Recent articles will provide a more detailed discussion on this subject than is possible within the scope of this chapter [145,146,147,148].

3.4.1 Cavity Ring-Down Spectroscopy

Cavity ring-down spectroscopy (CRDS) is a direct absorption technique, which can be performed with pulsed or continuous light sources. This technique was derived from the characterization process of high reflectors, in which the ring down rate indicated directly the reflectivity of the mirrors. Since the original demonstration for use in spectroscopic measurements [142], many papers have since reported the improvement and applicability of this technique and extended it to longer near-IR and mid-IR wavelengths [142,145,149,150,151,152,153,154,155]. Today, CRDS is used extensively in the visible and near infrared. In one example, a pulsed laser is employed for measurements of hydrogen-bonded clusters formed in molecular beams [156]. The progress in the mid-IR has been stimulated by the availability of ultra-low loss cavity mirrors and convenient mid-IR solid-state sources, such as pulsed quantum cascade laser and parametric conversion sources. With pulsed lasers, CRDS requires a short laser pulse to be injected into a high finesse optical cavity to produce a sequence of pulses leaking out through the end mirror from consecutive traversals of the cavity by the pulse. Typically, the laser pulse is short and has a small coherence length compared to a relatively large physical cavity length. Under these conditions interference effects are avoided and the intensity of the cavity pulses decays exponentially with a time constant

$$\tau = \frac{l}{c}\frac{1}{\alpha l - \ln R} \tag{7}$$

where α is the absorption coefficient of the intracavity medium, l is the cavity length and R is the mirror reflectivity (both mirrors are assumed to have the same reflectivity and the refractive index of the medium is assumed to be 1). By measuring the ring-down time, τ, without and with the absorbing gas present, the value of α can be determined. This technique is simple and immune to laser power fluctuations.

In the previous discussion, pulsed laser sources with low coherence length were considered and as a result of high-mirror reflectivities, the light levels reaching the detector are small. An alternative approach utilizes the resonance of the cavity by employing CW laser sources with a long coherence length. This is illustrated in the "wavenumber time domain" depicted in Fig. 8a. The laser line represented by the dashed curve is broader than the cavity mode spacing, or free spectral range $\mathrm{FSR} = c/2l$. The cavity throughput can be made much higher if the laser linewidth $\Delta\nu_{\mathrm{L}} \ll \mathrm{FSR}$. This condition can be satisfied if a narrow-line CW laser is used. When the laser frequency coincides with one of the cavity modes as shown in Fig. 8b, the cavity throughput is approximately $T = \Delta\nu_{\mathrm{C}}/\Delta\nu_{\mathrm{L}}$, where $\Delta\nu_{\mathrm{C}}$ is the spectral

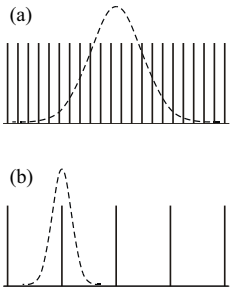

Fig. 8. Two situations of laser radiation filtering by an optical cavity (idealized one-dimensional consideration). (**a**) The laser linewidth is much broader than the cavity mode spacing (i.e. pulsed). In this case, the cavity throughput does not depend on the laser linewidth but is solely defined by the cavity finesse. (**b**) The laser linewidth is less than the cavity mode spacing. The cavity throughput is determined by the ratio of the cavity mode width to the laser linewidth

width of the cavity mode (1–10 kHz). The laser emission can be interrupted and the ring-down decay measured in the same manner as it is done with a pulsed laser. The use of CW laser sources for ring down was first proposed by *Lehmann* in 1996 [157], followed by *Romanini* et al. [158,159] using CW near-infrared DFB diode lasers. In order to maintain a good overlap of the laser with the cavity mode, the two must be locked to each other.

The first work on CRDS measurements with a QC-DFB laser was reported by *Paldus* et al. [160]. The authors used a CW laser generating 16 mW at $\lambda = 8.5\,\mu$m. The measured ring-down time of the empty three-mirror cavity was 0.93 μs. An acousto-optic modulator was used to interrupt the cavity injection for ring-down time measurements. The system was tested on diluted ammonia mixtures, and a noise-equivalent sensitivity of 0.25 ppbv achieved. An estimated $1.0 \times 10^{-9}\,\mathrm{cm}^{-1}$ detectable absorbance limit was reported. A spectroscopic gas sensor for nitric oxide (NO) detection at 5.2 μm based on CDRS was reported by *Kosterev* et al. [161]. Measurements of parts per billion (ppb) NO concentrations in N_2 with a 0.7 ppb standard error for an 8 s data acquisition time were performed. Interesting work [162,156] has been done combining a novel OPO with cavity ring-down spectroscopy.

A practical advantage of pulsed CRDS over CW CRDS is its applicability to study transient species formed for example by laser ablation sources [163].

3.4.2 Cavity-Enhanced Absorption Spectroscopy

A simpler (as compared to CDRS) method to exploit a high finesse optical cavity for increasing the sensitivity to absorption has been developed [164,165,166,167,168,169] and is called "integrated cavity output spectroscopy" (ICOS) or "cavity-enhanced absorption spectroscopy" (CEAS). Here, laser light is coupled into the high-finesse cavity via accidental coincidences of the light with the cavity eigenmodes by dithering the cavity length. The time-integrated intensity radiation leaking out of such an optical cavity, averaged over many cavity modes, can be used to determine the absorption of the intracavity medium. Effectively this is equivalent to a time integration of the ring-down curve. Just as in cavity ring-down spectroscopy, an effective optical pathlength of several kilometers can be obtained in a very small volume.

However, in its most simple configuration, the noise levels are relatively high since the cavity transmission varies significantly, depending on whether the laser is on or off resonance with the cavity. The ability to effectively average over these frequency response functions is the limiting noise factor to date. A novel approach by *Paul* et al. [167] uses an off-axis cavity alignment similar to the mirror configuration in astigmatic Herriott cells. This effectively lowers the FSR of the cavity and generates a very dense cavity mode spectrum. In fact, as the reentrant condition becomes longer (many multiple paths until the input beam again overlaps with the cavity beam) the mode spacing will become so dense that the cavity transmission will be almost independent of the laser wavelength. This effectively eliminates the requirement of any laser wavelength (as in CEAS) or cavity dither by a piezoelectric transducer (as in ICOS). However, this in turn also collapses the Fabry–Pérot condition and the transmission is significantly lowered and thus higher laser powers or more sensitive detectors may be needed. This technique has been demonstrated first in the visible wavelength region [167] and has been recently extended to the near-IR region for measurements of a variety of species (CH_4, C_2H_2, CO, CO_2, NH_3) and demonstrated sensitivities of up to $3 \times 10^{-11}\,\mathrm{cm}^{-1}\,\mathrm{Hz}^{-1/2}$ at 1.51 µm [170]. A minimum detectable concentration of 0.3 ppb (S/N = 3) of C_2H_2 at 50 Torr was obtained (1 s averaging time). This latest development demonstrates the ability of cavity enhanced spectroscopic techniques to achieve similar detection sensitivities as obtained with traditional multipass cell absorption spectroscopy. However, the true figure of merit for a real world measurement is the ability to replicate the same result when one samples a constant input concentration. Since low frequency noise sources from a variety of causes may also be important in the measurement process, the ability to replicate the same answer in many successive measurements can be far worse than the inherent sensitivity, and this will be further discussed in Sect. 4.1.

One of the most advanced methods, which utilize cavity enhancement is called "Noise-Immune Cavity-Enhanced Optical Heterodyne Spectroscopy" (NICE-OHMS) technique [171,172]. This technique combines the power of signal enhancement of cavity enhanced spectroscopy with the noise reduction of FM spectroscopy. In this technique, the laser frequency is locked to the frequency of a cavity mode. This method has the potential to provide shot-noise limited sensitivity with an effective pathlength determined by the cavity ringdown time. *Ma* et al. [171] reported a sensitivity of $10^{-14}\,\mathrm{cm}^{-1}$. This spectacular sensitivity is superior to that achieved with CRDS. To achieve such sensitivity, the laser requires active frequency stabilization below the kHz linewidth level, which is comparable or less than the spectral width of the cavity mode. In addition NICE-OHMS typically requires milli-Torr sample pressure, which effectively reduces the gas density by two orders of magnitude, and hence the effective minimum detectable concentration. High optical saturation (≈ 300 W of power inside the cavity) makes the Beer–Lambert ab-

sorption law no longer valid and hence the extraction of quantitative data difficult. The first implementation of this technique using a QC-DFB laser has been reported [173]. The NICE-OHMS approach is technically highly sophisticated and is only suitable for fundamental laboratory applications. The application and suitability of this technique for quantitative trace gas measurements has not yet been demonstrated.

3.5 Photoacoustic and Photothermal Spectroscopy (Signal Enhancement)

Photoacoustic spectroscopy (PAS) has found its principal use in sensitive trace gas detection. It is based on the photoacoustic effect, in which acoustic waves result from the absorption of radiation. In its application to laser spectroscopy, the laser beam impinges on a selected target gas in a specially designed cell [174,175,176,177,178,179,180,181,182,183].

In contrast with other mid-IR absorption techniques, PAS is an indirect technique in which the effect on the absorbing medium and not direct light absorption is detected. Light, from either pulsed or chopped CW laser sources produces a transient temperature rise in an absorbing medium via non-radiative relaxation processes, which then translates into a pressure change or sound wave as illustrated in Fig. 9. This is detected with a sensitive microphone(s). The acoustic signal is directly related to the concentration of the absorbing molecules in the cell. For CW laser sources, there are two modes of operation for PAS, either the exciting light can be modulated at a frequency away from any cell resonance or it can be adjusted to coincide with an acoustic resonant frequency. The in-resonance mode is usually employed with the low-power pump lasers to provide larger signals. However, precautions may be necessary to minimize changes of the instrument response due to the change of the speed of sound caused by temperature and gas compositional changes. PAS is ideally a background-free technique: the absorbing gas generates the signal, and in the absence of an absorbing gas there is no acoustic signal. In real PAS experiments, background signals

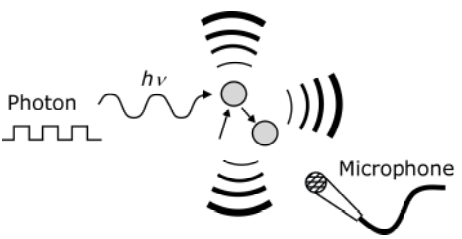

Fig. 9. Principle of photoacoustic spectroscopy. The incoming photons excite the target molecule at a resonant wavelength. Collisional de-excitation converts the absorbed energy into local heating and pressure waves, which can be detected by a microphone. (Illustration by courtesy of M. Webber, Pranalytica, Inc.)

can originate from nonselective absorption of the gas cell windows (coherent noise) and from outside acoustic (incoherent) noise, and from scattering of the laser radiation by aerosols onto the microphone. PAS signals are proportional to the pump laser intensity and therefore PAS is mostly used with high-power laser sources, in particular CO_2 and CO lasers [2,184]. In addition, diode (and in combination with high power optical fiber amplifiers) [185] and QC lasers, solid-state lasers, DFG and OPOs in the infrared have been applied to photoacoustic trace gas detection. Recently, a new approach called quartz enhanced PAS has been developed by *Kosterev* et al. [186]. Instead of using a gas-filled resonant acoustic cavity, the sound energy is accumulated in a high-Q crystal element. Feasibility experiments utilizing a quartz watch tuning fork demonstrate a sensitivity of $1.2 \times 10^{-7}\,\mathrm{cm}^{-1}\,\mathrm{W}/\sqrt{\mathrm{Hz}}$.

However, in trace gas monitoring applications, PAS is limited to extractive point monitoring due to the requirement of an absorption cell. In addition, PAS requires sufficient sampling pressures ($\approx 100\,\mathrm{Torr} - 1\,\mathrm{atm}$) for efficient collisional transfer and generation of the acoustic waves, thus limiting the selectivity in some cases. Furthermore, the effective collisional transfer can depend on the relative composition of the gas sample. For example, the deexcitation rates and hence the strength of the generated acoustic wave can differ by a factor of ≈ 2, as shown by Fried and Berg for the mid-IR detection of HCl under condition of dry samples and samples with 44 % relative humidity [187].

Another form of the photoacoustic effect is called photothermal absorption spectroscopy. Here, the photoacoustic signal is detected by means of recording the phase change in, for example, an unfolded Jamin interferometer. In this case, a non-resonant probe laser beam (e.g. He–Ne) is spatially overlapped with the resonant excitation beam (e.g. CO_2-laser). The probe beam is split and directed through a parallel path without the absorber. The modulated phase difference of these probe beams is measured [188]. Such a system has been configured for the detection of NH_3 and demonstrated a 2σ precision of 250 ppt and 31 ppt in a 1 s and 100 s integration time, respectively.

The key features of the photoacoustic technique include (1) excellent detection sensitivities down to sub-ppbv concentrations with powers in the watt range, (2) a large dynamic range, (3) PAS detector responsivity is almost independent of the pump wavelength, and (4) a PAS signal that is directly proportional to the absorbed radiation intensity, but does not scale with pathlength as with the previously discussed signal enhancement techniques. Indeed, the PAS signal will increase if a laser beam passes through the same volume/detection area of a microphone. However, it must pass through the same limited small interacting volume, otherwise more microphones are needed to be co-located along the laser path. Each added microphone will add to the noise floor. Therefore, only a moderate increase of the signal to

noise per unit $Hz^{-1/2}$ measurement time can be attained. On the other hand, the photothermal approach does scale linearly with pathlength.

Implementation of a QC-DFB laser to target fundamental absorptions has the potential of considerably improved flexibility and allows one to access many absorption features, whereas line-tunable CO_2 laser sources depend upon accidental overlap, and are restricted to the 9–11 μm region. Ammonia and water vapor photoacoustic spectra were obtained using a CW cryogenically cooled QC-DFB laser with a 16 mW power output at 8.5 μm as reported by *Paldus* et al. [189]. A PAS cell resonant at 1.66 kHz was used. The QC-DFB was used for frequency scans using temperature tuning and for real-time concentration measurements with a fixed laser temperature. Measured concentrations ranged from 2,200 ppmv to 100 ppbv. A detection limit of 100 ppbv ammonia ($\approx 10^{-5}$ noise-equivalent absorbance) at standard temperature and pressure was obtained for a 1 Hz bandwidth and a measurement interval of 10 min.

Recently, *Hofstetter* et al. [190] reported PAS measurements of ammonia, methanol and carbon dioxide using a pulsed 10.4 μm QC-DFB laser operated at 3–4 % duty cycle with 25 ns long current pulses (2 mW average power) and close to room temperature with Peltier cooling. Temperature tuning resulted in a wavelength range of $3\,cm^{-1}$with a linewidth of $0.2\,cm^{-1}$. This sensor used a 42 cm long PAS cell with a radial 16-microphone array for increased detection sensitivity. In addition the cell was placed between two concave reflectors resulting in 36 passes through the cell (with an effective pathlength of 15 m). The laser beam was mechanically chopped at a resonant cell frequency of 1.25 kHz, with a PAS signal enhancement by a Q factor of 70. A pyroelectric detector recorded the QC laser power to normalize the PAS signal. Detection of ammonia concentrations at the 300 ppbv level with a SNR of 3 was achieved at a pressure of 400 mbar.

4 Mid-Infrared Spectroscopic Applications

Tunable mid-infrared spectroscopic sources and spectroscopic techniques provide four important performance characteristics: sensitivity, selectivity, fast response time, and compactness. These are also based on similar optical component design and hence offer the unique ability to mix and match laser sources and techniques to be most useful for a given application. Recent progress in this field and growing optical industrial resources (e.g. optical fiber telecommunication) has led to the evolution and utilization of mid-IR spectroscopic techniques to a wide range of gas sensor applications. These include such diverse fields as: 1) environmental monitoring (CO, CO_2, CH_4 and CH_2O are important gas species in various aspects of atmospheric chemistry studies); 2) industrial emission measurements (e.g. fence line perimeter monitoring in the petrochemical industry, combustion sites, waste incinerators, down gas well monitoring, gas–pipe and compressor station safety);

3) urban (e.g. automobile traffic, power generation) and rural emissions (e.g. horticultural greenhouses, fruit storage and rice agro-ecosystems); 4) chemical analysis and control for manufacturing processes (e.g. in the semiconductor, pharmaceutical, and food industries); 5) detection of medically important molecules (e.g. NO, CO, CO_2, NH_3, C_2H_6 and CS_2), toxic gases, drugs, and explosives relevant to law enforcement and public safety; and 6) spacecraft habitat air-quality and planetary atmospheric science (e.g. such planetary gases as H_2O, CH_4, CO, CO_2 and C_2H_2).

4.1 Detailed Examples Using Selected Spectroscopic Sources and Techniques

There are literally hundreds of examples that can be cited where various mid-IR sources and spectroscopic techniques as discussed in the previous sections have been employed, including studies in the laboratory and industrial settings, and on ground-based, aircraft, balloon-borne, and rocket-borne platforms. Rather than cite examples of each, we present in this section three representative examples of spectroscopic sources utilizing lead-salt diode lasers, quantum cascade lasers, and difference-frequency generation coupled with either long-path and dual-beam absorption, wavelength modulation, or cavity-enhanced spectroscopy.

4.1.1 Lead-Salt Diode Laser Based Spectrometer for Airborne Atmospheric Chemistry Studies

In the following, we describe a lead-salt diode laser based trace gas sensor, which incorporates advances collectively developed by many research groups over the years, and thus illustrate the high performance that can be achieved routinely in a rugged airborne field setting. Aircraft measurements present unique and demanding challenges for one has to contend with: (1) changes in cabin temperature by as much as 20 °C over relatively short time periods of 1 h or less; (2) changes in cabin pressure by as much as 100 to 300 mbar over time periods of several minutes; (3) changes in system attitude; and (4) changes in aircraft vibrations that can couple beneficially or detrimentally into the system. As will be shown, by careful attention to numerous details, one can routinely measure absorbances as small as 0.7 to 1.7×10^{-6} for 1-min integration times employing pathlengths of 100 m on aircraft platforms.

Figure 10a illustrates the optical layout for a dual channel airborne spectrometer, which contains two Pb-salt diode lasers mounted in a liquid nitrogen dewar. Figure 10b shows a three-dimensional diagram of this system mounted in a temperature stabilized enclosure. This system has successfully acquired ambient measurements of the important atmospheric gas, formaldehyde (CH_2O), on numerous airborne campaigns. As shown, this system was also configured for simultaneous measurements of hydrogen peroxide (H_2O_2), another important atmospheric trace gas. The performance of this second

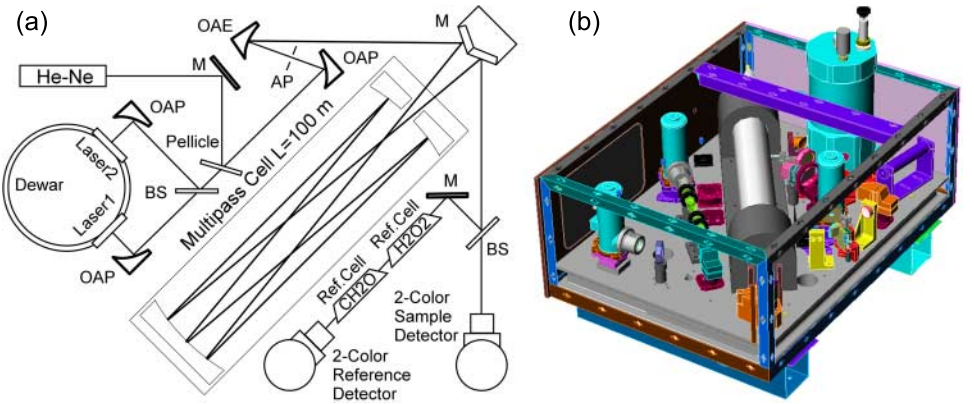

Fig. 10. (**a**) Optical set-up of a dual channel absorption laser spectrometer (DCALS); (**b**) three-dimensional digitally rendered model of DCALS configured for airborne operation

channel, however, was significantly inferior to that of the CH_2O channel, and will not be discussed here. Comprehensive details regarding the airborne system, the associated airborne measurements, as well as detailed background information on calibration, sampling, measurement accuracy, inlet tests, and ground-based and airborne comparisons studies can be found in *Fried* et al. [16] and references therein.

The IR radiation from the lead diode laser operating at 3.5 μm is directed through a multi-pass astigmatic Herriott cell (Aerodyne Research, Inc.) using a series of off-axis mirrors (two parabolic and one elliptical mirror), as shown in Fig. 10a. The IR beam, which traces out a Lissajous pattern in the cell, achieves a total optical pathlength of 100 m in a 3-l sampling volume. Upon exiting the cell, the IR beam is directed onto sample and reference indium-antimonide photovoltaic detectors. The optical system employs a minimum number of components, and of those, only two are readily adjustable. Each component, furthermore, is mounted on a rigid mount with as low a center height as possible. Both measures attempt to avoid subtle mechanical alignment changes. The entire optical enclosure, including the optical bench, is temperature stabilized to around 30 °C, typically to better than ±1 °C over time periods of many hours and significantly better than this over shorter time periods. A series of heaters mounted in the lid (not shown) are used for this purpose. Sheets comprised of an aluminum-balsa wood sandwich (partially removed in drawing) are mounted to the frame structure shown in Fig. 10b. These sheets provide both good thermal insulation and structural support. All the above precautions are critical for high performance aircraft measurements and are essential in extending the system stability period (to be discussed) out to 1-min and longer. Without temperature control, for example, one encounters rather significant changes in optical alignment,

background optical structure, and detector dark count signals, as the aircraft repeatedly ascends and descends throughout a typical flight pattern. In addition, owing to repeated changes in cabin pressure, it is equally critical to control the liquid-nitrogen pressure using some type of absolute pressure control valve. Without such control, the liquid-nitrogen boiling point would change, resulting in rather significant shifts in laser wavelength as the cryogen base temperature changes. Such temperature changes could also result in changes in dewar dimensions, and this may produce a consequent change in diode laser position which is integrally mounted to the dewar casing.

Absorption data are acquired using second harmonic detection coupled with sweep integration, as discussed by *Fried* et al. [12]. In this procedure, the diode laser wavelength is repetitively scanned across an isolated absorption feature of CH_2O (2831.6417 cm^{-1}) using a 200-point sawtooth ramp applied to the laser tuning current at a frequency of 50 Hz. A 50-kHz quasi-square wave modulation waveform is simultaneously applied to the laser tuning current, and the 2f signal at 100 kHz is detected using a digital lock-in amplifier. Second harmonic signals from the reference arm, which contains a high concentration cell of pure CH_2O, are treated identical to the sample arm. The lock-in amplifier outputs are then digitized (16-bit A/D converters) and co-averaged by a computer. The line center of the reference arm, which has very high signal-to-noise and serves as a wavelength reference, is determined on every scan. Each scan is then appropriately shifted in memory to align the peak centers before co-averaging. This fast spectral shifting is extremely important for high instrument performance [191]. Upon completion of each ambient measurement block, typically 60 s (3000 scans), the wavelength reference line center is determined using a polynomial fit, and an appropriate correction voltage is applied to the laser current controller to keep the absorption feature centered in the scan window. In addition, the mean value for the amplitude of each scan is forced through zero before co-averaging. This procedure effectively removes small scan-to-scan dc variability and thus improves the co-averaging effectiveness. The co-averaged spectrum at the end of each scan cycle is then transformed into the frequency domain employing an FFT algorithm, band pass filtered, and transformed back into the time domain. This approach helps to reduce both high and low frequency noise without significantly affecting the retrieved ambient signals.

By far the most dramatic improvement in instrument performance is achieved using rapid background subtraction. *Fried* et al. [15,12], *Zahniser* et al. [134], and *Werle* et al. [191] among others have presented the merits of this approach for tunable diode laser absorption spectroscopy. If carried out correctly, rapid background subtraction effectively captures and removes optical noise, which ultimately limits the performance of most if not all tunable diode laser instruments. As discussed previously, such noise is caused by light scattering from various optical elements, and this generates a somewhat random undulating background structure. Often such structure contains mul-

tiple frequencies, amplitudes, and time constants originating from multiple scattering sources. As addressed by *Werle* et al. [191], acquisition of sample and background spectra along with the associated cell flush times need to be accomplished within a characteristic system stability period, t_{opt}, in order for background subtraction to be effective. One can characterize this time period using the Allan variance, as first presented by *Werle* et al. [191] and subsequently by *Fried* et al. [12]. During time periods of constant optical enclosure temperature and constant pressure (not presently controlled in our airborne system), system stability periods typically range between 40 and 100 s before drifts become prevalent.

During airborne operation ambient air is drawn through a heated Teflon inlet at typical flow rates between 8 and 10 standard liters min^{-1} (slm, where standard conditions are defined as 273 K and 1 atmosphere pressure) and through the Herriott cell at sampling pressures around 40 Torr. Background spectra are acquired by passing ambient air from a second inlet through a heated Pd/Al_2O_3 scrubber, which removes CH_2O without significantly affecting the ambient water concentration, and this airflow is re-routed to the inlet tip at flow rates exceeding the sample flow. During a typical sampling sequence[16], six successive 10 s ambient spectra are acquired, and each 1 min ambient sampling block is preceded and followed by a 10 s background acquisition. An appropriate delay period of 9 s ($\approx$ 5 inlet/cell e-folding residence times) is employed after each switch before data are acquired. The backgrounds surrounding each 1 min block are averaged (time weighted) and subtracted point by point from each of the 10 s ambient spectra. The average laser power is determined for each 1 min sampling block using a third data acquisition channel to continuously record the sample detector dc voltage. The detector dark voltage is obtained every few 1-minute ambient cycles by blocking the laser beam with a shutter for a few seconds. The laser power is determined from the difference of the two measurements, and the ratio of the laser power obtained during calibration to that during a sample measurement is applied. Calibration spectra are typically acquired every 30–60 min by adding CH_2O standards, from a permeation calibration system, to the zero airflow near the inlet entrance. At the cell flows employed, typical CH_2O standard concentrations of 12–14 parts-per-billion by volume (ppbv) are generated at the Herriott cell entrance. Periodically, 7 ppbv standards are also added on top of ambient to check for inlet loss and to check the veracity of the data retrieval algorithm. Each 10 s background-subtracted ambient spectrum is fitted in real time to a background-subtracted calibration spectrum (acquired for 20 s) employing a multiple linear regression approach [192,193]. Each complete ambient acquisition cycle, which includes the acquisition of a 10 s background, 1 minute of ambient averaging, two 9 s delay periods and computer-processing overhead, typically takes 90 s, and this typically falls within the system stability period.

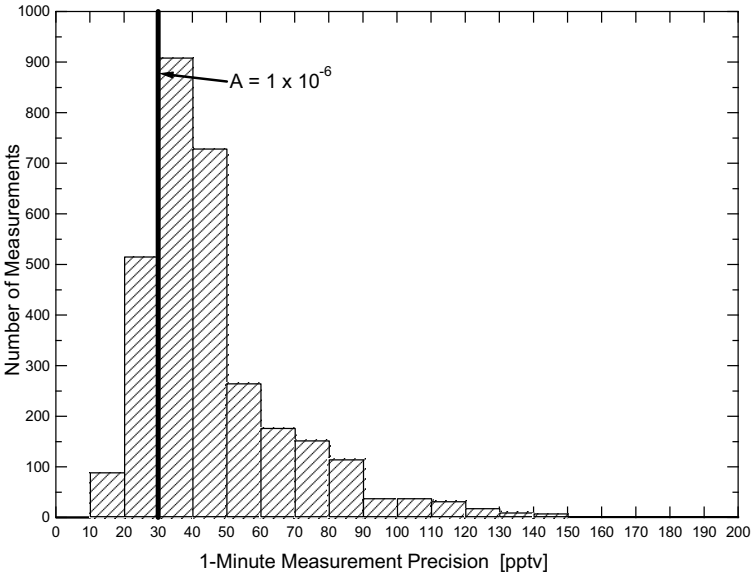

Fig. 11. Formaldehyde (CH_2O) measurement precision diagram at the 1σ level for airborne measurements throughout the TOPSE campaign [16]

Figure 11 shows the instrument performance obtained during the TOPSE (Tropospheric Ozone Production about the Spring Equinox) airborne campaign [16]. Here the 1-minute (1σ) measurement precision, obtained from the standard deviation of replicate measurements upon sampling relatively constant and low ambient CH_2O levels, is given in terms of a histogram. The histogram reflects the fact that the measurement precision during airborne operation is somewhat variable, depending upon the exact alignment stability and the degree to which the acquired backgrounds truly represent the actual backgrounds underlying the ambient spectra. As the real precision for any technique will vary, even in a laboratory setting, the histogram approach gives a more realistic assessment of overall instrument performance than a single figure of merit often reported for many techniques.

In addition, the results of Fig. 11 are obtained from replicate measurements, and not the precision of any given measurement, which in the case of tunable diode laser measurements, can be expressed in terms of an individual fit precision. As discussed by *Fried* et al. [12] this fit precision is proportional to the square root of the fit deviations, and in most instances was found to be a factor of 3 to 4 too optimistic. In this case, like that for many other techniques, there are additional sources of variance, which produce ambient results that have larger run-to-run variability than the precision of any individual measurement. Thus, from these two standpoints the results of Fig. 11 truly represent the meaningful performance that is obtain-

able with an airborne tunable diode laser system. As can be seen, most of the 1 min measurements (which require 90 s to acquire) yield 1σ replication precisions in the 20–50 pptv concentration range (median value = 40 pptv) for CH_2O during airborne operation. Employing a sampling pressure of 40 Torr, a temperature of 303 K, a 100 m pathlength, an integrated absorption cross-section of $5.44 \times 10^{-20}\,\mathrm{cm^2\,cm^{-1}molecule^{-1}}$ and an air-broadening coefficient of $0.107\,\mathrm{cm^{-1}\,atm^{-1}}$, one calculates using a Voigt function that a line center absorbance of 1×10^{-6} equates to a CH_2O concentration of 30 pptv. Thus the precisions above correspond to minimum detectable line center absorbances of 0.7 to 1.7×10^{-6}. This in turn computes to pathlength-normalized values of 7×10^{-11} to $1.7 \times 10^{-10}\,\mathrm{cm^{-1}}$ employing a 90 s sampling sequence.

4.1.2 Quantum-Cascade Laser Based Trace Gas Sensors in the Life Sciences

Laser spectroscopy is finding increasing applications in medicine and the life sciences [194,195,196,197,198,199]. A particular role for spectroscopy is in the monitoring of small molecules that have been shown to be important. The role of simple molecules such as nitric oxide (NO) in physiological processes has received considerable attention in recent years and was a subject of the 1998 Nobel Prize in Medicine.

One application is the measurement of NO in human breath samples, since exhaled air is an indicator of several processes taking place in the human body, in particular in assessing the severity of airway inflammation [200]. To observe NO in breath, a cavity-enhanced absorption spectroscopy (CEAS) sensor [169] with a CW QC-DFB laser operating at 5.2 µm with an output power of 80 mW was used. A direct performance comparison was carried out between a sensor configuration where the CES optical cavity was replaced with a 100 m pathlength multi-pass cell. It was found that in spite of having an effective pathlength of 670 m, CES had a lower absorption sensitivity because of baseline noise of $\approx 1\,\%$ (averaging 10^4 QC laser scans). These baseline fluctuations are intrinsic to CES and result from the mode structure of the cavity transmission spectrum. Some improvement in the CES baseline noise can be achieved with the recently developed off-axis ICOS technique [167].

In [161] a spectroscopic gas sensor for NO detection based on a cavity ring-down technique is described. NO is the major oxide of nitrogen formed during high-temperature combustion as well as an important nitrogen-containing species in the atmosphere (NO is a precursor of smog and acid rain). NO is also involved in a number of vital physiological processes, and its detection in human breath has potential applications (e.g. as a marker for diseases like asthma or inflammatory processes) in noninvasive medical diagnostics. A CW QC-DFB laser operating at 5.2 µm was used as a tunable single-frequency light source. The technique used consists of the following features:

1) The laser frequency is slowly scanned across the absorption line of interest.
2) One of the cavity mirrors is dithered back and forth to ensure periodic, random coincidences of the laser frequency with a cavity mode.
3) Once such a resonance occurs and the cavity is filled, the laser beam entering the cavity is abruptly interrupted or set off-resonance, and the decay rate of the exiting light is measured.

From (7) in Sect. 3.4, the absorption coefficient can be determined as

$$\alpha = \frac{1}{c}\left(\frac{1}{\tau} - \frac{1}{\tau_{\text{empty}}}\right) \tag{8}$$

where τ_{empty} is the decay constant of the cavity without absorber.

The sensor schematic is shown in Fig. 12. It depicts a simpler design than the first CRDS experiment with a QC-DFB laser described in [160]. In that work a variable temperature cryostat for laser frequency tuning was used with the inherent complexity and additional cost of an acousto-optic modulator (AOM) to interrupt the QC laser beam. In the work reported in [161] both frequency tuning and the laser emission interruption were realized by manipulation of the QC laser pump current. No active temperature control was applied to the QC-DFB laser located in a liquid nitrogen optical cryostat: The laser current was supplied by a low-noise current source and monitored using the 0.5 Ω resistor denoted by r_1 in Fig. 12. The laser frequency was tunable from 1922.9 to 1920.8 cm^{-1} when the pump current changed from 300 mA (lasing threshold) to 660 mA. At higher current levels the laser emission was multimode. The tuning range permitted NO detection by accessing absorption lines at 1921.599 cm^{-1} and 1921.601 cm^{-1} (R(13.5) components of

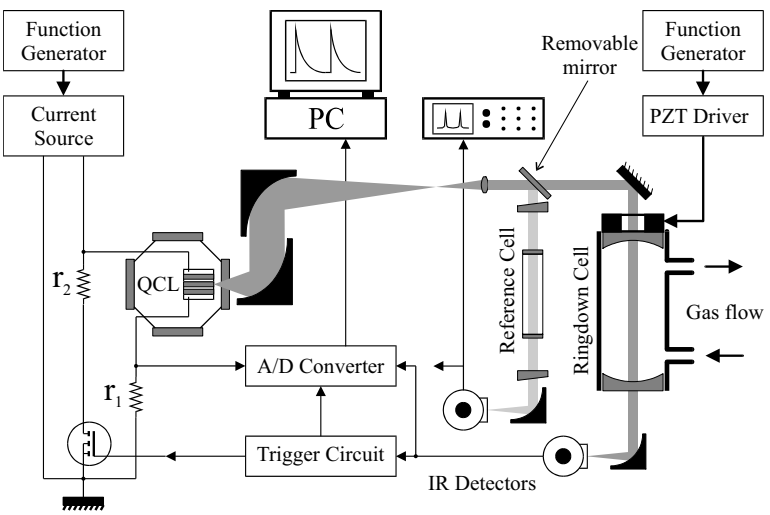

Fig. 12. Schematic of a QC laser based cavity ring-down spectrometer [161]

the fundamental absorption band). Absorption lines of water vapor and CO_2 were also observed. The $\boldsymbol{l} = 37\,\mathrm{cm}$ long, linear high-finesse optical cavity was formed by two concave mirrors with a 6 m radius of curvature. The measured ring-down time of the cavity without absorber was $\tau \approx 3.5\,\mu\mathrm{s}$, corresponding to $\Delta\,\nu_{\mathrm{C}} \approx 45\,\mathrm{kHz}$. The laser linewidth was estimated to be $\Delta\,\nu_{\mathrm{L}} = 3\,\mathrm{MHz}$.

When a certain level of the detector signal was reached signaling that a TEM_{00} cavity mode is coupled to the laser, a triggering circuit (TC) opened a metal-oxide semiconductor field-effect transistor (MOSFET) to shunt the laser current, thereby reducing it to a subthreshold value. At the same time, the TC triggered an analog–digital converter, and the detector signal showing the cavity ring-down was digitized for $\approx 30\,\mu\mathrm{s}$ and stored in computer memory. The MOSFET was kept open for $35\,\mu\mathrm{s}$, so that the laser radiation would not interfere with measurements of the cavity decay constant. This triggering-and-acquisition process was repeated and consecutive ring-down transients were stacked in the A/D memory until a desired number of transients was acquired. The results were post-processed to fit each transient with an exponential decay function yielding a ring-down time $\boldsymbol{\tau}$. The inverse ring-down time plotted as a function of the laser current provides the absorption spectrum. An example of the NO absorption in a mixture with pure N_2 is presented in Fig. 13. The noise-equivalent sensitivity was estimated to be 0.7 ppbv for an 8 s data acquisition time. It was not possible to use this sensor directly for measurements of NO concentration in exhaled air ($\approx$ 10 ppbv) because of strong CO_2 interference, which can be avoided if the appropriate NO absorption line is chosen (e.g. like R(7.5) components at 1903.123 and $1903.134\,\mathrm{cm}^{-1}$) with a QC laser that accesses this wavelength.

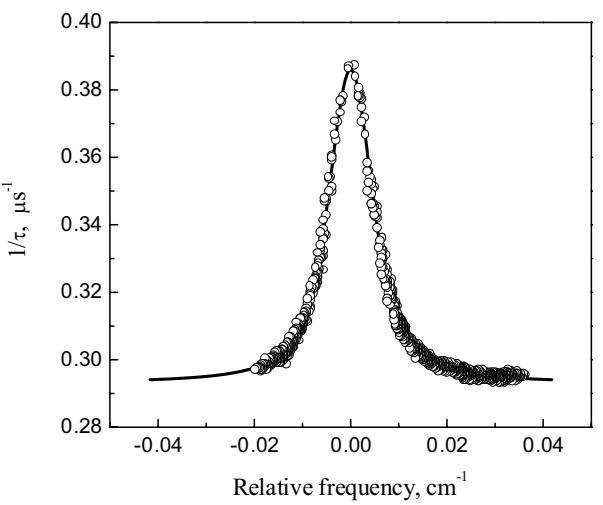

Fig. 13. NO absorption in a mixture with pure N_2 obtained with the sensor depicted in Fig. 12

Recent work indicates that other gases, such as carbon monoxide (CO), can also play a very significant physiological role. CO is produced from heme catabolism by the enzyme heme oxygenase. Previous work has shown that CO promotes blood flow by inhibiting vascular tone and platelet aggregation and that neuronal CO production may modulate the NO-cGMP (guanosine 3′, 5′-cyclic monophosphate) signaling system, demonstrating important biochemical interactions between the two diatomic gases. The extremely low levels of gas production in living cells and the relatively short *in vivo* lifetime of cell cultures have complicated detailed understanding of the kinetic, or time-dependent processes responsible for their generation. A typical production rate of CO, for example from vascular smooth muscle cells (VSMCs), is 1 to 10 pmol/min/10^7 cells. Instrumentation for *in vivo* measurement of gas production should have sensitivities on the parts per billion (ppb) level in order that the dynamics of gas production can be followed with laboratory-scale cell sample populations [201]. Because of low CO production rates from biological tissues, measurements of CO concentrations have been limited to gas chromatography and radioisotope counting techniques. Although these methods are highly sensitive, they cannot measure CO directly, requiring several time-consuming intermediate steps requiring $\approx$ 15 min, and may be affected by interference from water, oxygen, and carbon dioxide.

Infrared laser absorption spectroscopy is an attractive alternative approach for the detection of biological CO at the parts-per-billion (ppb) level in real time [202,203]. A compact gas sensor measured endogenenous CO production from vascular cells using a mid-IR spectroscopic laser source based on differencefrequency generation (DFG) of two near-IR lasers. The CO absorption was detected in the fundamental vibration band near 4.6 μm. In this work, an extractive technique was used with gas samples taken from the flask containing the cell culture to an 18 m pathlength optical multi-pass cell so that the measurements could be performed at a reduced pressure of 100 Torr.

Kosterev et al. [203] reported an improved design and performance of an optical mid-IR CO sensor intended for continuous monitoring of cell culture activity at ambient atmospheric pressure. The same fundamental absorption band region was used for CO detection, but a pulsed quantum cascade laser with a distributed feedback structure (QC-DFB) [25] was employed instead of the DFG source. The high output power of the QC-DFB laser and an advanced data analysis approach made it possible to detect biological CO and CO production rates with $\approx$ 1 m optical pathlength folded above a standard culture flask of VSMCs.

A further improvement of the pulsed QC-DFB based sensor was reported by *Kosterev* et al. [204]. The laser beam was split into two channels, one being used to probe the gas absorption and the other as a reference to measure the laser pulse energy. The subsequent normalization eliminated pulse-to-pulse energy fluctuations as an error source, which was the predominant cause of error previously [203]. This automated sensor was used for contin-

uous monitoring of CO in ambient air detected by its R(3) absorption line at 2158.300 cm^{-1} ($\lambda \approx 4.6\,\mu m$). A noise-equivalent detection limit of 12 ppbv was experimentally demonstrated with a 1 m optical pathlength. This sensitivity corresponds to a standard error in fractional absorbance of 3×10^{-5}.

All the measurements were carried out at atmospheric pressure, and hence it was not possible to periodically acquire a baseline with an evacuated sample container. In order to keep the baseline (which included weak unwanted interference fringes from optical elements) stable during multi-hour measurements, the slow drifts of the laser frequency were actively compensated by computer-controlled corrections to the subthreshold current. A constant CO production rate of 44 ppbv/hour was observed, taking into account the 0.5 liter volume of the cell culture container. This corresponds to a net CO production rate of 0.9 nmol/10^7 cells/hour, which is in agreement with previous measurements [202] obtained with similar cells and treatment regimes.

A compact mobile ammonia sensor based on a thermoelectrically cooled pulsed QC-DFB laser operating at $\approx 10\,\mu m$ was described in [205]. High sensitivity detection of NH_3 is also of interest in the control of deNO_x chemistry, industrial safety and medical diagnostics of kidney related diseases. The optical configuration of this sensor was similar to that described in [206], but the multi-pass cell was replaced with a simple 50 cm long double pass gas cell, and no zero air subtraction employed. The laser housing was improved by replacing the previous beam-shaping optical system consisting of two off-axis parabolic mirrors and a lens with a single aspheric lens. The laser was scanned over two absorption lines of the NH_3 fundamental ν_2 band. The sensor was completely automated and only required the LN_2 dewar of the detector to be refilled every 12 h. This sensor was applied to the continuous monitoring of NH_3 concentration levels at the ppm level present in bioreactor vent gases in a water reprocessing system located at NASA's Johnson Space Center in Houston, TX. A sensitivity of better than 0.3 ppmv was estimated which was sufficient to quantify expected ammonia levels of 1 to 10 ppmv.

4.1.3 Design and Applications of Fiber Based Difference Frequency Based Mid-IR Gas Sensors

In the following, the optical architecture and performance of several field portable gas sensors based on difference frequency sources are discussed. The gas sensors described here utilize fiber based near-IR lasers, high-power rare earth doped fiber amplification and single-pass difference-frequency generation in QPM-PPLN crystals (Sect. 1.2).

Difference frequency generation utilizing optical fiber coupled and fiber based pump sources allows great flexibility in designing a robust mid-infrared source with power levels typically ranging from 0.1 mW to 1 mW. Figure 14a depicts four representative fiber based DFG-source configurations, which have been developed and applied to trace gas detection. In order to evaluate and

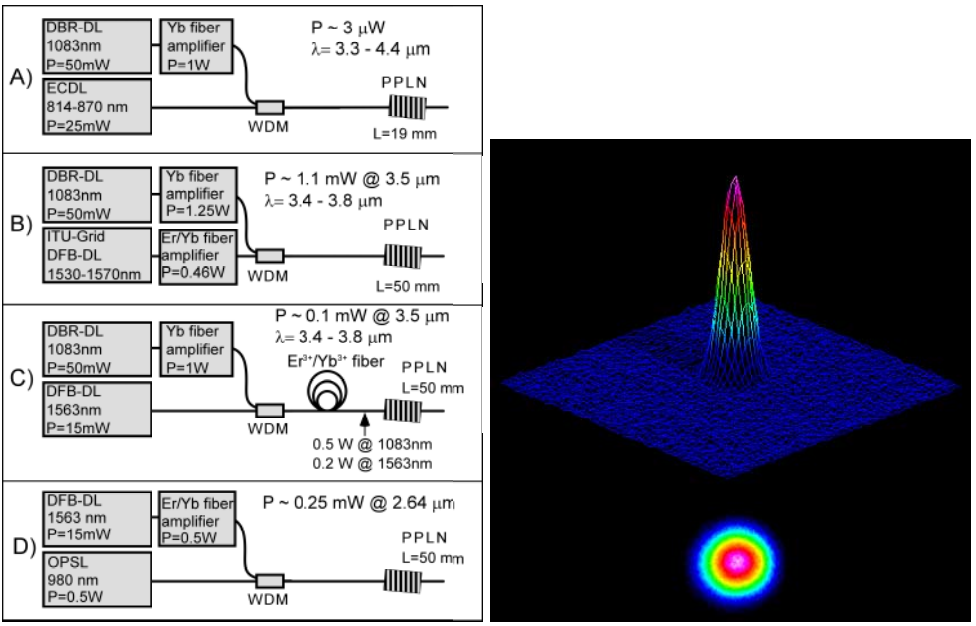

Fig. 14. (**a**) Fiber based difference-frequency generation sources using narrow-linewidth diode laser sources and high-power optical fiber amplifiers. Shown are respective wavelengths, input and generated power levels [207]. (**b**) Optical fiber pumped DFG beam profile: measured 37.5 cm from PPLN exit facet, beam diameter @ $1/e^2$: $x = 0.80\,\text{mm}$, $y = 0.80\,\text{mm}$ Gaussian fit $> 95\,\%$ [208]

confirm robust performance of these sources itself and their applicability, direct long-pathlength absorption as the simplest form of sensitive detection was used. Advanced signal enhancing techniques and noise reduction techniques have been applied and laboratory results indicate unique advantages of these sources.

In the examples shown, low-power seed diode laser sources are used in combination with high-power, wide bandwidth fiber amplifiers. Several inexpensive low-power diode laser sources whose wavelengths overlap with the gain region of the fiber optic amplifier can be used, one at a time, or can also be multiplexed to be amplified simultaneously or sequentially in time. This permits easy modification of a fixed optical fiber platform by choosing any desirable seed wavelength within the fiber amplifier(s) gain bandwidth in the difference frequency mixing process and generate the desired mid-IR wavelength(s) (Fig. 1). Fiber amplifiers retain the spectroscopic properties of the seed laser sources, and thus decouple the high-power requirement for efficient DFG from low-noise, narrow-linewidth operation. This approach is more cost effective and technically easier than constructing a pump laser source which meets all of the three requirements at the same time, namely

narrow-linewidth, high-power (W), and multiple-wavelength operation. In addition, near-IR diode lasers have similar tuning rates with current and temperature. This in turn provides predictable ease of exchange of sources and mid-IR frequency stabilization. For example, an ambient temperature change will introduce the same wavelength shift to two near IR diode laser sources with similar tuning rates and use of similar types of current/temperature controller. If those laser sources are difference-frequency mixed, the drift is subtractive and affords high inherent mid-IR wavelength stability, provided the diode lasers and controllers are carefully selected and operate at the same ambient conditions. The use of fiber optics for DFG pump beam delivery also provides a stable and inherent spatial overlap to produce a circular, homogeneous beam with a near-Gaussian intensity distribution as shown in Fig. 14b. This offers small beam sizes ($\approx 2\,\mathrm{mm}$) with $\mathrm{f}/\# \approx 100$, and are obtained by the use of only one relay optical element to collect and image the DFG beam to the spectroscopic cell (e.g. multi-pass cell).

Quasi-phase matched periodically poled $LiNbO_3$ (QPM-PPLN) has been shown to be efficient for parametric frequency down conversion (see Sect. 1.2). It also offers flexibility in the conversion bandwidth by either using crystals incorporating multiple QPM periods or a fan-out design for continuous QPM [69].

The DFG sources depicted in Fig. 14a have been used in several field applications to demonstrate their feasibility in real-world environments. These include remote volcanic gas measurements in Nicaragua, operation in an industrial setting and analysis of a space rated trace contaminant control system (using the source shown in Fig. 14a A) [209,210]. The DFG source depicted in Fig. 14a B), shown in more detail in Fig. 15, is configured for high sensitivity dual-beam long-path absorption spectroscopy of urban pollutants.

Using this source, *Rehle* et al. [211] conducted extensive urban gas detection of CH_2O over extended time periods and achieved a detection limit of 0.32 ppbv of atmospheric formaldehyde at $3.53\,\mu\mathrm{m}$ ($2832\,\mathrm{cm}^{-1}$). This corresponds to a sensitivity of $1 \times 10^{-9}\,\mathrm{cm}^{-1}$ in combination with a 100 m path-length low-volume (3.3 l) astigmatic mirror Herriott gas cell. A dual-beam absorption configuration that employs two dc-coupled Peltier-cooled HgCdTe (MCT) detectors was used to eliminate the optical interference fringes originating from the refractive optical elements of the DFG conversion stage and optical fiber components. A typical absorption spectrum obtained is shown in Fig. 16. To further enhance the signal-to-noise, mainly limited by electronic noise and technical noise from the multi-pass cell, wavelength modulation and zero-background subtraction could be used as described in the lead-salt diode laser based detection system above. However, these techniques were not used with this device, because of relatively high urban formaldehyde concentrations ranging from 1 to 50 ppbv. The sensor as shown in Fig. 15 has been operated autonomously for a continuous nine and five-day period at two separate field sites in the Greater Houston area, administered by

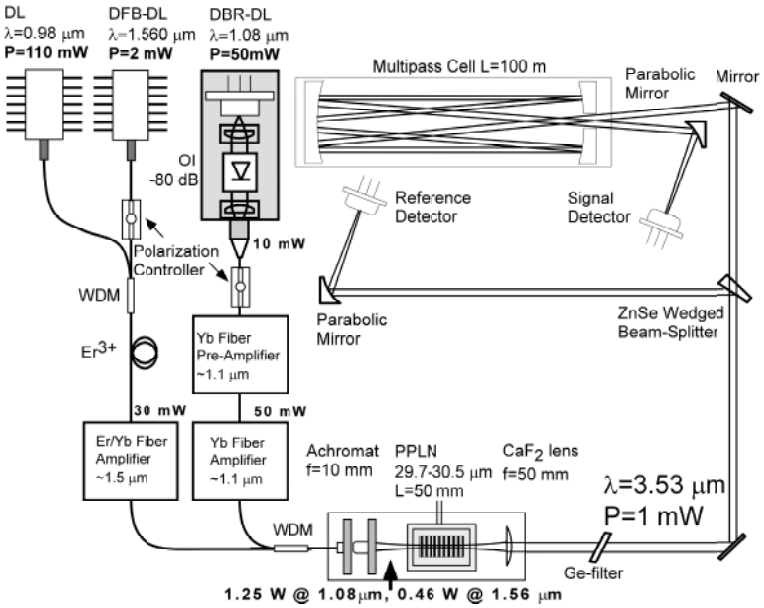

Fig. 15. High-power continuous-wave DFG source employing dual-beam spectroscopy used for urban pollution monitoring of CH_2O. DL, diode laser; DFB-DL, distributed feedback-DL; DBR-DL, distributed Bragg reflector-DL; OI, optical isolator; WDM, wavelength division multiplexer

the Texas Natural Resource Conservation Commission (TNRCC) and the Houston Regional Monitoring Corporation (HRM). The acquired spectroscopic data were compared with results obtained by a well-established wet-chemical *o*-(2,3,4,5,6-pentafluorobenzyl) hydroxylamine (PFBHA) technique with good agreement. While the accuracy of the determined concentrations is comparable with results from conventional wet-chemical techniques, the described DFG sensor offers excellent time resolution on the order of seconds and permits unattended continuous operation for long periods of time. The maintenance-free design of a tunable infrared DFG based diode laser spectrometer and the capability of remotely controllable computerized operation makes such instrumentation a convenient, robust tool for mobile trace gas detection. Thus, formaldehyde concentration measurements using direct absorption laser spectroscopy have proved to be a sensitive and effective method for online trace gas monitoring in an urban setting. Further testing of a similar DFG system by *Richter* et al. [208] utilizing additional wavelength modulation spectroscopy and zero air background subtraction has generated laboratory based replicate detection precisions (1σ, 1 min average) of better than $2.5 \times 10^{-10}\,\mathrm{cm}^{-1}$, which corresponds to 74 pptv minimal detectable CH_2O concentration.

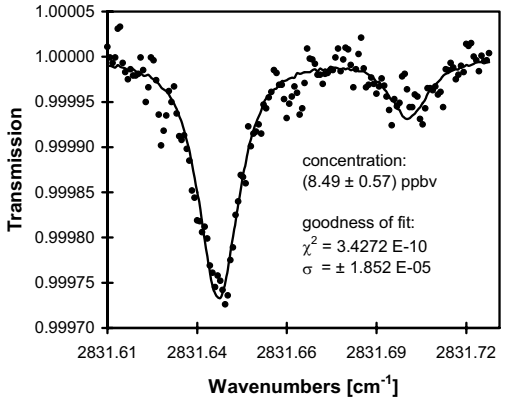

Fig. 16. Absorption spectra of CH_2O using the DFG based gas sensor depicted in Fig. 15

The recent rapid advances in the optical fiber telecommunication industry has produced a number of new laser sources and components to continuously expand the DFG wavelength coverage and generate higher mid-IR power at the mW level. Many of the requirements for telecom applications overlap and directly enhance the spectroscopic performance of DFG based mid-IR sources. These include narrower linewidth ($< 1\,\mathrm{MHz}, 1\,\mathrm{s}$), stable higher power using highly saturated two-stage fiber amplifiers, and wavelength stability. Relatively simple, yet powerful, mid-IR sources can be designed. Fig. 14a D) shows the optical design of an all telecom wavelength based mid-IR source [212]. Here, an optically pumped VCSEL operating at 980 nm provides over 500 mW coupled into a single-mode optical fiber with linewidths of $\approx 10\,\mathrm{MHz}$. The other DFG pump source is a standard low noise and narrow-linewidth ($< 1\,\mathrm{MHz}$) DFB diode laser amplified by a 500 mW Er/Yb fiber amplifier. Mid-IR powers in excess of 0.25 mW at 2.64 µm are easily obtained with this DFG mixing configuration in combination with a 2 cm long QPM-PPLN crystal. Using this source, spectroscopic detection of fundamental absorption lines of hydrogen fluoride (HF) has been performed. Employing direct absorption spectroscopy, fractional absorption sensitivities of 1×10^{-4} was obtained. The DFG frequency stability of this source was measured by tracking a high resolution HF absorption line over several hours, which indicated a maximum peak-to-peak wavelength drift of 20 MHz during a 2 h time interval. Given the strong absorption cross-section of HF at this wavelength range ($S = 1 \times 10^{-18}\,\mathrm{cm\ molecule}^{-1}$), sub-ppb detection sensitivity can be obtained over relatively short pathlengths of several meters.

The spectroscopic performance characteristics of DFG sources and their inherent flexibility to access specific fundamental mid-IR absorption lines can be further facilitated for precision ratio measurements of, for example, isotopic $^{12}CO_2/^{13}CO_2$. The ability of measuring isotopic ratios with a high

precision and selectivity makes this technique particularly attractive for a variety of applications, such as carbon cycle research, volcanic gas emission studies, and the use of isotopic tracers in medical diagnostics. In order to be useful, measurement precisions of $0.18^0/_{00}$ to $1^0/_{00}$ are required and are defined as $[(R_{\text{sample}} - R_{\text{std}})/R_{\text{std}}] \times 1000$, where $R = [^{13}CO_2]/[^{12}CO_2]$. Isotopic ratios can be measured by detection of closely paired absorption lines of $^{12}CO_2/^{13}CO_2$ found for example in the 4.3 micron wavelength range and comparing this spectroscopic signatures with a known reference gas. To obtain high precision, several key requirements of the source and spectroscopic technique have to be addressed. Most important are the inherent stability and measurement precision of absorption spectra and the temperature dependence of the probed absorption lines. Closely paired absorption lines of $^{12}CO_2/^{13}CO_2$ with similar absorption strengths usually originate from different ground energy levels and hence have different temperature dependences. Figure 17 shows three suitable line pairs for the detection of $^{12}CO_2/^{13}CO_2$ isotopic ratios. Also indicated are the temperature coefficients based on the Boltzman distribution [213].

Using the DFG source depicted in Fig. 14a A) in combination with a single-pass 20 cm long dual chamber absorption cell, *Erdelyi* et al. [214] have obtained a 1σ measurement precision of $\approx 0.8^0/_{00}$. The dual chamber absorption cell was built from a solid piece of brass and incorporated two parallel small bore extrusions and was end-fitted with common Brewster angle windows. This allowed rapid comparison measurements of sample gases with

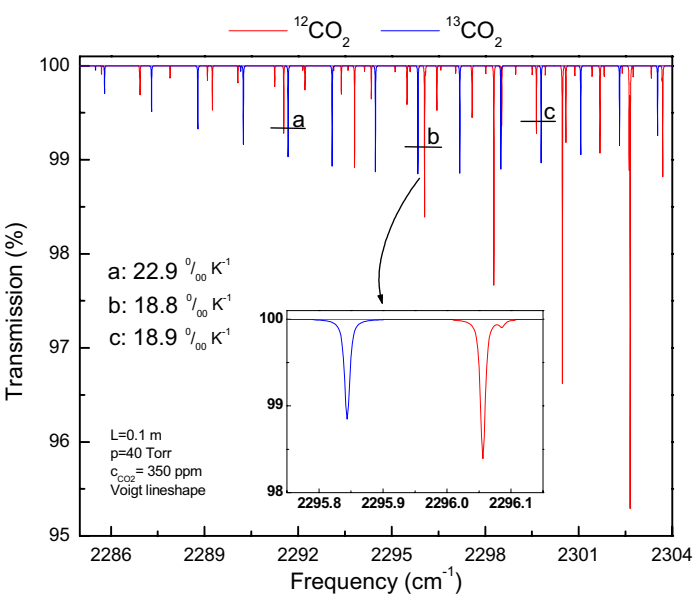

Fig. 17. HITRAN simulation of isotopic CO_2 lines

a known reference gas mixture. The cell design also ensured good thermal mixing of the sample and reference gas standard and because of the small volume, a minimal amount of expensive reference gases. The measurement precision of this system was mainly limited by electronic noise due to low pump power from an ECDL operating at the edge of its tuning range, and in turn only provided a mid-IR power of $\approx 0.2\,\mu$W. However, the achieved precision is sufficient for many applications including volcanic gas emission studies. Other approaches with similar detection levels ranging from $0.2^0/_{00}$ to $2^0/_{00}$ have been reported in the literature, including lead-salt diode, color-center-, CO_2-, and near-IR diode laser sources in combination with various multi-pass cell designs and cavity enhanced spectroscopy [213,215,216,217,218].

5 Summary and Outlook

This chapter has attempted to survey the current status of various tunable CW solid-state laser based sources and techniques suitable for mid-infrared laser applications in spectroscopy. The emphasis of our discussion has been to acquaint the reader with the key fundamentals and options in realizing optimized performance, different available sensitivity enhancement schemes and minimum detectable absorbances (10^{-4} to 10^{-6}). Wherever possible, we tried to elucidate the factors that are important for real-world sensors and applications. In this regard we presented three representative examples of laser sources, techniques and their specific applications. Each of these critical areas will constantly undergo incremental improvements of the underlying enabling technologies and lead to further advances in *in situ* and remote gas sensing techniques.

Reliable mid-IR sources in combination with cavity-enhanced spectroscopy and optical fiber technologies will improve detection limits. These new technologies and approaches will also lead to new effective sensor configurations. For example, one could imagine the use of low-loss single mode fibers with high reflective coatings employed as a ring down cavity and combined with evanescent field absorption of a partially stripped fiber. These potential and other new inventions will improve the simplicity, the cost and robustness of spectroscopic laser based gas sensors and broaden their range of applications [219,220,221].

As these new laser sources and spectroscopic techniques evolve in maturity, an emphasis on the instrument replicate sensitivity and precision of quantitative trace gas detection must be given, because it is the unequivocal merit of usefulness in many applications. Such issues may not solely depend on the laser or measurement principle employed, but also on numerous other factors which may be application dependent, such as ambient temperature and pressure conditions. It will thus be important to address these important key factors without increasing the system complexity. Such spectroscopic

laser based systems will have a large impact on the means and quality with which we can sense the world around us.

Acknowledgements

The authors would like to thank Dr. Douglas S. Baer (Los Gatos Research, Inc.), Dr. James F. Kelly (Pacific Northwest National Laboratories), Dr. Anatoliy A. Kosterev and Dr. Robert F. Curl (Rice University), and Dr. Michael E. Webber (Pranalytica, Inc.) for their helpful ideas, comments and invaluable scientific discussions during the preparation of this manuscript.

References

1. L. R. Narasimhan, W. Goodman, C. K. N. Patel: Correlation of breath ammonia with blood urea nitrogen and creatinine during hemodialysis, Proc. National Acad. Sci. **98**, 4617–4621 (2001) 447
2. M. E. Webber, M. Pushkarsky, C. K. N. Patel: Fiber-amplifier enhanced photoacoustic spectroscopy using near-infrared tunable diode lasers, Appl. Opt. **42**, 2119–2126 (2003) 447, 479
3. J. Reid, D. T. Casidy, R. T. Menzies: Linewidth measurements of tunable diode lasers using heterodyne and étalon techniques, Appl. Opt. **21**, 3961–3965 (1982) 448
4. S. Lundqvist, J. Margolis, J. Reid: Measurements of pressure-broadening coefficients of NO and O_3 using a computerized tunable diode laser spectrometer, Appl. Opt. **21**, 3109–3113 (1982) 448
5. R. L. Sams, A. Fried: Microphone triggering circuit for elimination of mechanically induced frequency-jitter in diode laser spectrometers: implications for quantitative analysis, Appl. Opt. **26**, 3552–3558 (1987) 448
6. R. Sams, A. Fried: Potential sources of systematic errors in tunable-diode-laser absorption measurements, Appl. Spectrosc. **40**, 24–29 (1986) 449
7. H. Preier, Z. Feit, J. Fuchs, D. Kostyk, W. Jalenak, J. Sproul: Status of lead-salt diode laser development at spectra-physics, in *Monitoring of Gaseous Pollutants by Tunable Diode Lasers*, Proc. Int. Symposium, Freiburg, Germany (1988), G. S. R. Grisar, M. Tacke, G. Restelli (Eds.) (Kluwer Academic, Dordrecht 1989) pp. 85–102 449
8. D. L. Wall, J. C. Sproul, Z. Feit, G. W. Sachse: Development of IR tunable diode lasers and source assemblies for atmospheric monitoring and related applications, in *Tunable Diode Laser Spectroscopy, Lidar, and DIAL Techniques for Environmental and Industrial Measurements*, A. Fried, D. K. Killinger, H. I. Schiff (Eds.) (SPIE, Atlanta, GA 1993) pp. 2–11 449
9. M. Tacke: Recent results in lead-salt laser development at the IPM, in *Monitoring of Gaseous Pollutants by Tunable Diode Lasers*, Proc. Int. Symposium, Freiburg, Germany (1988), G. S. R. Grisar, M. Tacke, and G. Restelli (Eds.) (Kluwer Academic, Dordrecht 1989) pp. 103–118 449
10. R. Grisar: *Monitoring of Gaseous Pollutants by Tunable Diode Lasers*, Proc. Int. Symposium, Freiburg, Germany (1991) (Kluwer Academic, Dordrecht 1992) 449

11. D. J. Brassington: Tunable diode laser absorption spectroscopy for the measurement of atmospheric species, in *Advances in Spectroscopy*, R. E. Hester (Ed.) (John Wiley, New York 1995) pp. 83–148 449
12. A. Fried, B. Henry, B. Wert, S. Sewell, J. R. Drummond: Laboratory, ground-based, and airborne tunable diode laser systems: performance characteristics and applications in atmospheric studies, Appl. Phys. B **67**, 317–330 (1998) 449, 483, 484, 485
13. P. Werle: A review of recent advances in semiconductor laser-based gas monitors, Spectrochim. Acta **54**, 197–236 (1998) 449
14. A. Fried, S. McKeen, S. Sewell, J. Harder, B. Henry, P. Goldan, W. Kuster, E. Williams, K. Baumann, R. Shetter, C. Cantrell: Photochemistry of formaldehyde during the 1993 tropospheric OH photochemistry experiment, J. Geophys. Res. Atmospheres **102**, 6283–6296 (1997) 450
15. A. Fried, S. Sewell, B. Henry, B. P. Wert, T. Gilpin, J. R. Drummond: Tunable diode laser absorption spectrometer for ground-based measurements of formaldehyde, J. Geophys. Res. Atmospheres **102**, 6253–6266 (1997) 450, 483
16. A. Fried, Y. Wang, C. Cantrell, B. Wert, J. Walega, B. Ridley, E. Atlas, R. Shetter, B. Lefer, M. T. Coffey, J. Hannigan, D. Blake, N. Blake, S. Meinardi, B. Talbot, J. Dibb, E. Scheuer, O. Wingenter, J. Snow, B. Heikes, D. Ehhalt: Tunable diode laser measurements of formaldehdye during the TOPSE 2000: Distributions, trends, and model comparisons, J. Geophys. Res. **108**, D4, 8365 (2003) 450, 453, 482, 484, 485
17. A. N. Baranov, Y. Cuminal, G. Boissier, C. Alibert, A. Joullié: Low-threshold laser diodes based on type-II GaInAsSb/GaSb quantum-wells operating at 2.36 μm at room temperature, Electron. Lett. **32**, 2279–2280 (1996) 451
18. Y. Rouillard, F. Genty, A. Perona, A. Vicet, D. A. Yarekha, G. Boissier, P. Grech, A. N. Baranov, C. Alibert: Edge and vertical surface emitting lasers around 2.0–2.5 μm and their applications, Philos. Trans. R. Soc. London A **359**, 581–597 (2001) 451
19. J. C. Nicolas, A. N. Baranov, Y. Cuminal, Y. Rouillard, C. Alibert: Tunable diode laser absorption spectroscopy of carbon monoxide around 2.35 μm, Appl. Opt. **37**, 7906–7911 (1998) 451
20. B. Lane, D. Wu, A. Rybaltowski, H. Yi, J. Diaz, M. Razeghi: Compressively strained multiple quantum well InAsSb lasers emitting at 3.6 μm grown by metal-organic chemical vapor deposition, Appl. Phys. Lett. **70**, 443–445 (1997) 451
21. P. Werle, A. Popov: Application of antimonide lasers for gas sensing in the 3–4-μm range, Appl. Opt. **38**, 1494–1501 (1999) 451
22. P. Werle, R. Mucke, F. D'Amato, T. Lancia: Near-infrared trace-gas sensors based on room-temperature diode lasers, Appl. Phys. B **67**, 307–315 (1998) 451
23. P. Werle: Spectroscopic trace gas analysis using semiconductor diode lasers, Spectrochim. Acta A **52**, 805–822 (1996) 451
24. T. C. Hasenberg, R. H. Miles, A. R. Kost, L. West: Recent advances in Sb-based midwave-infrared lasers, IEEE J. Quant. Electron. **33**, 1403–1406 (1997) 451
25. F. Capasso, C. Gmachl, R. Paiella, A. Tredicucci, A. L. Hutchinson, D. L. Sivco, J. N. Baillargeon, A. Y. Cho, H. C. Liu: New frontiers in quan-

tum cascade lasers and applications, IEEE J. Sel. Topics Quant. Electron. **6**, 931–947 (2000) 451, 489
26. C. Gmachl, A. Straub, R. Colombelli, F. Capasso, D. L. Sivco, A. M. Sergent, A. Y. Cho: Single-mode, tunable distributed-feedback and multiple-wavelength quantum cascade lasers, IEEE Quantum Electron. **38**, 569–581 (2002) 451
27. C. Gmachl, F. Capasso, D. L. Sivco, A. Y. Cho: Recent progress in quantum cascade lasers and applications, Rep. Prog. Phys. **64**, 1533–1601 (2001) 451
28. R. M. Williams, J. F. Kelly, J. S. Hartman, S. W. Sharpe, M. S. Taubman, J. L. Hall, F. Capasso, C. Gmachl, D. L. Sivco, J. N. Baillargeon, A. Y. Cho: Kilohertz linewidth from frequency-stabilized mid-infrared quantum cascade lasers, Opt. Lett. **24**, 1844–1846 (1999) 451, 452
29. M. Beck, D. Hofstetter, T. Aellen, J. Faist, U. Oesterle, M. Ilegems, E. Gini, H. Melchior: Continuous wave operation of a mid-infrared semiconductor laser at room temperature, Science **295**, 301–305 (2002) 452
30. R. Kohler, C. Gmachl, A. Tredicucci, F. Capasso, D. L. Sivco, S. N. G. Chu, A. Y. Cho: Single-mode tunable, pulsed, and continuous wave quantum-cascade distributed feedback lasers at lambda congruent to 4.6–4.7 μm, Appl. Phys. Lett. **76**, 1092–1094 (2000) 452
31. J. Faist, D. Hofstaetter, M. Beck, T. Aellen, M. Rochat, S. Laser: Bound-to-continuum and two-phonon resonance quantum cascade lasers for high duty cycle, high temperature operation, IEEE J. Quant. Electron. **38**, 533–546 (2002) 452
32. M. S. Taubman, T. L. Myers, B. D. Cannon, R. M. Williams, F. Capasso, C. Gmachl, D. L. Sivco, A. Y. Cho: Frequency stabilization of quantum-cascade lasers by use of optical cavities, Opt. Lett. **27**, 2164–2166 (2002) 452
33. H. Q. Le, G. W. Turner, J. R. Ochoa, M. J. Manfra, C. C. Cook, Y. H. Zhang: Broad wavelength tunability of grating-coupled external cavity mid-infrared semiconductor lasers, Appl. Phys. Lett. **69**, 2804–2806 (1996) 452
34. G. P. Luo, C. Peng, H. Q. Le, S. S. Pei, W. Y. Hwang, B. Ishaug, J. Um, J. N. Baillargeon, C. H. Lin: Grating-tuned external-cavity quantum-cascade semiconductor lasers, Appl. Phys. Lett. **78**, 2834–2836 (2001) 452, 453
35. K. G. Libbrecht, J. L. Hall: A low noise high-speed diode laser controller, Rev. Sci. Instrum. **64**, 2133 (1993) 452
36. R. Q. Yang, J. L. Bradshaw, J. D. Bruno, J. T. Pham, D. E. Wortman: Mid-infrared type-II Interband cascade lasers, IEEE Quantum Electron. **38**, 559–568 (2002) 453
37. G. P. Luo, C. Peng, H. Q. Le, S. S. Pei, H. Lee, W. Y. Hwang, B. Ishaug, J. Zheng: Broadly wavelength-tunable external cavity mid-infrared quantum cascade lasers, IEEE J. Quant. Electron. **38**, 486–494 (2002) 453
38. D. D. Nelson, M. S. Zahniser, J. B. McManus, C. E. Kolb, J. L. Jimenez: A tunable diode laser system for the remote sensing of on-road vehicle emissions, Appl. Phys. B **67**, 433–441 (1998) 453
39. D. E. Cooper, C. B. Carlisle: High-sensitivity FM spectroscopy with a lead-salt diode laser, Opt. Lett. **13**, 719–721 (1988) 454
40. L. F. Mollenauer, White, J. C.: General principles and some common features, in *Tunable Lasers*, L. F. Mollenauer, White, J. C. (Eds.) (Springer, Berlin Heidelberg 1987) pp. 1–18 454

41. P. F. Moulton: Tunable solid-state lasers, Proc. IEEE **80**, 348–364 (1992) 454
42. N. P. Barnes, F. Allario: Tunable solid-state lasers: an emerging technology for remote sensing of planetary atmospheres, Proc. SPIE **868**, 107–116 (1988) 454
43. S. Kück: Laser-related spectroscopy of ion-doped crystals for solid-state lasers, Applied Physics B-Lasers & Optics B **72**, 515–562 (2001) 454
44. A. Sennaroglu, A. O. Konca, C. R. Pollock: Continuous-wave power performance of a 2.47-μm Cr^{2+}: ZnSe laser: Experiment and modeling, IEEE J. Quant. Electron. **36**, 1199–1205 (2000) 454
45. I. T. Sorokina, E. Sorokin, A. Di Lieto, M. Tonelli, R. H. Page, K. I. Schaffers: Efficient broadly tunable continuous-wave Cr^{2+}: ZnSe laser, J. Opt. Soc. Am. B **18**, 926–930 (2001) 454
46. S. Schiller, J. Mlynek: Special Issue, Continuous-wave optical parametric oscillators, materials, devices, applications, Appl. Phys. B **66**, 664–764 (Springer, Berlin, Heidelberg 1998) 455
47. P. E. Powers, T. J. Kulp, S. E. Bisson: Continuous tuning of a continuous-wave periodically poled lithium niobate optical parametric oscillator by use of a fan-out grating design, Opt. Lett. **23**, 59–61 (1998) 455
48. R. J. Lang, D. G. Mehyus, D. F. Welch: External cavity, continuously tunable wavelength source, US patent no. 5,771,252 (1998) 456
49. A. T. Schremer, C. L. Tang: External-cavity semiconductor laser with 1000 GHz continuous piezoelectric tuning range, IEEE Photon. Technol. Lett. **2**, 3–5 (1990) 456
50. D. Wandt, M. Laschek, K. Przyklenk, A. Tünnermann, H. Welling: External cavity laser diode with 40 nm continuous tuning range around 825 nm, Opt. Commun. **130**, 81–84 (1996) 456
51. T. Kiguchi, A. Uematsu, M. Kitano, H. Ogura: Grating external cavity diode lasers with broad tunable range and narrow spectral linewidth for high-resolution spectroscopy, Jap. J. Appl. Phys. **35**, 5890–5895 (1996) 456
52. B. Pezeshki: New approaches to laser tuning, Opt. Photon. News **12**, 34–38 (2001) 456
53. L. A. Coldren: Monolithic tunable diode lasers, IEEE J. Sel. Topics Quant. Electron **6**, 988–999 (2000) 456
54. B. Schmidt, S. Illek, R. Gessner, M. C. Amann: Design and realization of a buried-heterostructure tunable-twin-guide laser diode with electrical blocking regions, IEEE J. Quant. Electron. **35**, 794–802 (1999) 456
55. G. Morthier, B. Moeyersoon, R. Baets: A lambda/4-shifted sampled or superstructure grating widely tunable twin-guide laser, IEEE Photon. Technol. Lett. **13**, 1052–1054 (2001) 456
56. H. Ishii, H. Tanobe, F. Kano, Y. Tohmori, Y. Kondo, Y. Yoshikuni: Broad-range wavelength coverage (62.4 nm) with superstructure-grating DBR laser, Electron. Lett. **32**, 454–455 (1996) 456
57. E. T. Wetjen, D. M. Sonnenfroh, M. G. Allen, T. F. Morse: Demonstration of a rapidly tuned Er^{3+}-doped fiber laser for sensitive gas detection, Appl. Opt. **38**, 3370–3375 (1998) 457
58. H. Simonsen, J. Henningsen, S. Sogaard, J. E. Pedersen: CO_2 stabilized Er^{3+}-doped fibre laser at 1578 nm, Eur. Frequency Time Forum (EFTF) (2000) 457

59. I. Freitag, A. Tünnermann, H. Welling: Power scaling of monolithic miniature Nd:YAG ring lasers to output powers of several watts, Opt. Commun. **115**, 511 (1995) 457
60. D. Boucher, W. Chen, J. Burie, P. Peze: A novel CW optical laser-based difference-frequency infrared spectrometer, Ann. Phys. (Paris) **23**, 247–248 (1998) 457
61. W. D. Chen, J. Burie, D. Boucher: Investigation on infrared laser absorption spectroscopy measurement of acetylene trace quantities, Infrared Phys. Technol. **41**, 339–348 (2000) 457
62. W. Schade, T. Blanke, U. Willer, C. Rempel: Compact tunable mid-infrared laser source by difference frequency generation of two diode-lasers, Appl. Phys. B **63**, 99–102 (1996) 457
63. M. Seiter, M. W. Sigrist: Trace-gas sensor based on mid-IR difference-frequency generation in PPLN with saturated output power, Infrared Phys. Technol. **41**, 259–269 (2000) 457
64. D. Lee, T. Kaing, J. J. Zondy: An all-diode-laser-based, dual-cavity $AgGaS_2$ CW difference-frequency source for the 9–11 µm range, Appl. Phys. B **67**, 363–367 (1998) 457, 459
65. H. D. Kronfeldt, G. Basar, B. Sumpf: Application of a CW tunable infrared spectrometer based on difference-frequency generation in $AgGaS_2$ for self-broadening investigations of NO at 5 µm, J. Opt. Soc. Am. B **13**, 1859–1863 (1996) 457
66. M. Seiter, D. Keller, M. W. Sigrist: Broadly tunable difference-frequency spectrometer for trace gas detection with noncollinear critical phase-matching in $LiNbO_3$, Appl. Phys. B **67**, 351–356 (1998) 457
67. M. Seiter, M. W. Sigrist: Compact gas sensor using a pulsed difference-frequency laser spectrometer, Opt. Lett. **24**, 110–112 (1999) 457
68. D. G. Lancaster, A. Fried, B. Wert, B. Henry, F. K. Tittel: Difference-frequency-based tunable absorption spectrometer for detection of atmospheric formaldehyde, Appl. Opt. **39**, 4436–4443 (2000) 457, 459
69. D. Richter, D. G. Lancaster, F. K. Tittel: Development of an automated diode-laser-based multicomponent gas sensor, Appl. Opt. **39**, 4444–4450 (2000) 457, 459, 461, 492
70. W. D. Chen, F. Cazier, F. Tittel, D. Boucher: Measurements of benzene concentration by difference-frequency laser absorption spectroscopy, Appl. Opt. **39**, 6238–6242 (2000) 457, 459
71. D. G. Lancaster, D. Richter, F. K. Tittel: Portable fiber-coupled diode-laser-based sensor for multiple trace gas detection, Appl. Phys. B **69**, 459–465 (1999) 457, 459
72. U. Simon, F. K. Tittel: Nonlinear optical frequency conversion techniques, in *Atomic, Molecular, and Optical Physics: Electromagnetic Radiation*, R. Celotta, R. G. Hulet, F. B. Dunning (Eds.), Experimental Methods in the Physical Sciences **29**, 231–278 (Academic Press, New York 1997) 457
73. A. S. Pine: Doppler-limited molecular spectroscopy by difference-frequency mixing, J. Opt. Soc. Am. **64**, 1683–1690 (1974) 458
74. B. Sumpf, D. Rehle, T. Kelz, H. D. Kronfeldt: A tunable diode-laser spectrometer for the MIR region near 7.2 µm applying difference-frequency generation in $AgGaSe_2$, Applied Physics B-Lasers & Optics **67**, 369–373 (1998) 459

75. P. A. Budni, L. A. Pomeranz, M. L. Lemons, C. A. Miller, J. R. Mosto, E. P. Chicklis: Efficient mid-infrared laser using 1.9-μm-pumped Ho:YAG and $ZnGeP_2$ optical parametric oscillators, J. Opt. Soc. Am. B **17**, 723–728 (2000) 459
76. W. C. Eckhoff, R. S. Putnam, S. X. Wang, R. F. Curl, F. K. Tittel: A continuously tunable long-wavelength CW IR source for high-resolution spectroscopy and trace-gas detection, Appl. Phys. B **63**, 437–441 (1996) 459
77. W. Chen, G. Mouret, D. Boucher: Difference-frequency laser spectroscopy detection of acetylene trace constituent, Appl. Phys. B **67**, 375–378 (1998) 459
78. R. S. Putnam, D. G. Lancaster: Continuous-wave laser spectrometer automatically aligned and continuously tuned from 11.8 to 16.1 μm by use of diode-laser-pumped difference-frequency generation in GaSe, Appl. Opt. **38**, 1513–1522 (1999) 459
79. W. K. Burns, W. McElhanon, L. Goldberg: Second harmonic generation in field poled, quasi-phase matched, bulk $LiNbO_3$, IEEE Photon. Technol. Lett. **6**, 252–254 (1994) 459
80. L. E. Myers: Periodically poled materials for nonlinear optics, in *Advances in Lasers and Applications*, D. M. Finlayson, B. D. Sinclair (Eds.) (Scottish Univ. Science Press, 1999) pp. 141–180 459
81. K. Fradkin-Kashi, A. Arie, P. Urenski, G. Rosenman: Mid-infrared difference-frequency generation in periodically poled $KTiOAsO_4$ and application to gas sensing, Opt. Lett. **25**, 743–745 (2000) 459
82. K. Fradkin, A. Arie, A. Skliar, G. Rosenman: Tunable midinfrared source by difference frequency generation in bulk periodically poled $KTiOPO_4$, Appl. Phys. Lett. **74**, 914–916 (1999) 459
83. K. Fradkin-Kashi, A. Arie: Multiple-wavelength quasi-phase-matched nonlinear interactions, IEEE J. Quant. Electron. **35**, 1649–1656 (1999) 459
84. S. Sanders, R. J. Lang, L. E. Myers, M. M. Fejer, R. L. Byer: Broadly tunable mid-ir radiation source based on difference frequency mixing of high power wavelength-tunable laser diodes in bulk periodically poled $LiNbO_3$, Electron. Lett. **32**, 218–219 (1996) 459
85. W. Chen, G. Mouret, D. Boucher, F. K. Tittel: Mid-infrared trace gas detection using continuous-wave difference frequency generation in periodically poled $RbTiOAsO_4$, Appl. Phys. B **72**, 873–876 (2001) 459
86. D. Mazzotti, P. De Natale, G. Giusfredi, C. Fort, J. A. Mitchell, L. W. Hollberg: Difference-frequency generation in PPLN at 4.25 μm: an analysis of sensitivity limits for DFG spectrometers, Appl. Phys. B **70**, 747–750 (2000) 459
87. O. Levi, T. J. Pinguet, T. Skauli, L. A. Eyeres, K. R. Parameswaran, J. S. Harris, Jr., M. M. Fejer, T. J. Kulp, S. E. Bisson, B. Gerard, E. Lallier, L. Becouarn: Difference frequency generation of 8-micron radiation in orientation-patterned GaAs, Opt. Lett. **27**, 2091–2093 (2002) 459
88. D. G. Lancaster, D. Richter, R. F. Curl, F. K. Tittel: Real-time measurements of trace gases using a compact difference-frequency-based sensor operating at 3.5 μm, Appl. Phys. B **67**, 339–345 (1998) 459
89. D. G. Lancaster, L. Goldberg, J. Koplow, R. F. Curl, F. K. Tittel: Fibre coupled difference frequency generation utilising ytterbium-doped fibre amplifier and periodically poled $LiNbO_3$, Electron. Lett. **34**, 1345–1347 (1998) 459

90. D. G. Lancaster, D. Richter, R. F. Curl, F. K. Tittel, I. Goldberg, J. Koplow: High-power continuous-wave mid-infrared radiation generated by difference frequency mixing of diode-laser-seeded fiber amplifiers and its application to dual-beam spectroscopy, Opt. Lett. **24**, 1744–1746 (1999) 459
91. D. G. Lancaster, R. Weidner, D. Richter, F. K. Tittel, J. Limpert: Compact CH_4 sensor based on difference frequency mixing of diode lasers in quasi-phasematched $LiNbO_3$, Opt. Commun. **175**, 461–468 (2000) 459
92. D. Richter, D. G. Lancaster, R. F. Curl, W. Neu, F. K. Tittel: Compact mid-infrared trace gas sensor based on difference-frequency generation of two diode lasers in periodically poled $LiNbO_3$, Appl. Phys. B **67**, 347–350 (1998) 459
93. D. Richter, M. Erdelyi, F. K. Tittel: Ultra-compact mid-IR spectroscopic source based on frequency converted Yb-Er/Yb fiber amplified CW diode lasers, in C. Marshall (Ed.): *Adv. Solid-State Lasers*, OSA Trends Opt. Photon. **50** (Opt. Soc. Am., Washington, DC 2001) pp. 96–100 459
94. J. J. Zondy: The effects of focusing in type-I and type-II difference-frequency generations, Opt. Commun. **149**, 181–206 (1998) 460
95. T. Topfer, K. P. Petrov, Y. Mine, D. Jundt, R. F. Curl, F. K. Tittel: Room-temperature mid-infrared laser sensor for trace gas detection, Appl. Opt. **36**, 8042–8049 (1997) 460
96. M. H. Chou, M. A. Arbore, M. M. Fejer: Adiabatically tapered periodic segmentation of channel waveguides for mode-size transformation and fundamental mode excitation, Opt. Lett. **21**, 794–796 (1996) 460
97. M. H. Chou, K. R. Parameswaran, M. M. Fejer, I. Brener: Multiple-channel wavelength conversion by use of engineered quasi-phase-matching structures in $LiNbO_3$ waveguides, Opt. Lett. **24**, 1157–1159 (1999) 460
98. K. P. Petrov, A. T. Ryan, T. L. Patterson, L. Huang, S. J. Field, D. J. Bamford: Mid-infrared spectroscopic detection of trace gases using guided-wave difference-frequency generation, Appl. Phys. B **67**, 357–361 (1998) 460
99. K. P. Petrov, A. P. Roth, T. L. Patterson, T. P. S. Thoms, L. Huang, A. T. Ryan, D. J. Bamford: Efficient difference-frequency mixing of diode lasers in lithium niobate channel waveguides, Appl. Phys. B **70**, 777–782 (2000) 460
100. D. Hofmann, G. Schreiber, C. Haase, H. Herrmann, W. Grundkotter, R. Ricken, W. Sohler: Quasi-phase-matched difference-frequency generation in periodically poled Ti:$LiNbO_3$ channel waveguides, Opt. Lett. **24**, 896–898 (1999) 460
101. P. E. Powers, T. J. Kulp, S. E. Bisson: Continuous tuning of a continuous-wave periodically poled lithium niobate optical parametric oscillator by use of a fan-out grating design, Opt. Lett. **23**, 159–161 (1998) 461, 462
102. G. M. Gibson, M. H. Dunn, M. J. Padgett: Application of a continuously tunable, CW optical parametric oscillator for high-resolution spectroscopy, Opt. Lett. **23**, 40–42 (1998) 461, 462
103. T. J. Edwards, G. A. Turnbull, M. H. Dunn, M. Ebrahimzadeh, H. Karlsson, G. Arvidsson, F. Laurell: Continuous-wave singly resonant optical parametric oscillator based on periodically poled $RbTiOAsO_4$, Opt. Lett. **23**, 837–839 (1998) 461, 462
104. E. V. Kovalchuk, D. Dekorsy, A. I. Lvovsky, C. Braxmaier, J. Mlynek, A. Peters, S. Schiller: High-resolution Doppler-free molecular spectroscopy with a continuous-wave optical parametric oscillator, Opt. Lett. **26**, 1430–1432 (2001) 461, 462

105. R. Altahtamouni, K. Bencheikh, R. Storz, K. Schneider, M. Lang, J. Mlynek, S. Schiller: Long-term stable operation and absolute frequency stabilization of a doubly resonant parametric oscillator, Appl. Phys. B **66**, 733–739 (1998) 461, 462
106. M. E. Klein, D. H. Lee, J. P. Meyn, B. Beier, K. J. Boller, R. Wallenstein: Diode-pumped continuous-wave widely tunable optical parametric oscillator based on periodically poled lithium tantalate, Opt. Lett. **23**, 831–833 (1998) 461, 462
107. G. A. Turnbull, M. H. Dunn, M. Ebrahimzadeh: Continuous-wave, intracavity optical parametric oscillators – an analysis of power characteristics, Appl. Phys. B **66**, 701–710 (1998) 461
108. W. R. Bosenberg, A. Drobshoff, J. I. Alexander, L. E. Myers, R. L. Byer: Continuous-wave singly resonant optical parametric oscillator based on periodically poled $LiNbO_3$, Opt. Lett. **21**, 713–715 (1996) 462
109. L. E. Myers, R. C. Eckardt, M. M. Fejer, R. L. Byer, W. R. Bosenberg: Multigrating quasi-phase-matched optical parametric oscillator in periodically poled $LiNbO_3$, Opt. Lett. **21**, 591–593 (1996) 462
110. L. E. Myers, W. R. Bosenberg: Periodically poled lithium niobate and quasi-phase-matched optical parametric oscillators, IEEE J. Quant. Electron. **33**, 1663–1672 (1997) 462
111. F. Hanson, P. Poirer, M. A. Arbore: Single-frequency mid-infrared optical parametric oscillator source for coherent laser radar, Opt. Lett. **26**, 1794–1796 (2001) 462
112. M. A. Arbore, M. M. Fejer: Singly resonant optical parametric oscillation in periodically poled lithium niobate waveguides, Opt. Lett. **22**, 151–153 (1997) 462
113. A. J. Henderson, P. M. Roper, L. A. Borschowa, R. D. Mead: Stable, continuously tunable operation of a diode-pumped doubly resonant optical parametric oscillator, Opt. Lett. **25**, 1264–1266 (2000) 462
114. M. van Herpen, S. te Lintel Hekkert, S. E. Bisson, F. J. M. Harren: Wide single-mode tuning of a 3.0–3.8 μm, 700 mW continuous-wave Nd:YAG-pumped optical parametric oscillator based on periodically poled lithium niobate, Opt. Lett. **27**, 640–642 (2002) 462
115. S. Schiller, K. Schneider, J. Mlynek: Theory of an optical parametric oscillator with resonant pump and signal, J. Opt. Soc. Am. B **16**, 1512–1524 (1999) 462
116. U. Strossner, J. P. Meyn, R. Wallenstein, P. Urenski, A. Arie, G. Rosenman, J. Mlynek: Single-frequency continuous-wave optical parametric oscillator system with an ultrawide tuning range of 550 to 2830 nm, J. Opt. Soc. Am. B **19**, 1419–1424 (2002) 462
117. L. S. Rothman, C. P. Rinsland, A. Goldman, S. T. Massie, D. P. Edwards, J. M. Flaud, A. Perrin, C. Camypeyret, V. Dana, J. Y. Mandin, J. Schroeder, A. McCann, R. R. Gamache, R. B. Wattson, K. Yoshino, K. V. Chance, K. W. Jucks, L. R. Brown, V. Nemtchinov, P. Varanasi: The HITRAN molecular spectroscopic database and hawks (HITRAN atmospheric workstation) 1996 edn., J. Quant. Spectrosc. Radiat. Transfer **60**, 665–710 (1998) 463, 466, 472
118. N. Jacquinet-Husson, E. Arie, J. Ballard, A. Barbe, G. Bjoraker, B. Bonnet, L. R. Brown, C. Camy-Peyret, J. P. Champion, A. Chedin, A. Chursin, C. Clerbaux, G. Duxbury, J. M. Flaud, N. Fourrie, A. Fayt, G. Graner, R. Gamache,

A. Goldman, V. Golovko, G. Guelachvili, J. M. Hartmann, J. C. Hilico, J. Hillman, G. Lefevre et al.: The 1997 spectroscopic GEISA databank, J. Quant. Spectrosc. Radiat. Transfer **62**, 205–254 (1999) 463, 466
119. J. Humlicek: An efficient method of evaluation of the complex probability function: the Voigt function and its derivatives, J. Quant. Spectrosc. Radiat. Transfer **21**, 309 (1979) 466
120. U. Platt: Air monitoring by differential optical absorption spectroscopy, in *Encyclopedia of Analytical Chemistry*, L. E. Myers (Ed.) (Wiley, Chichester 2000) pp. 1936–1959 467
121. S. Svanberg: *Atomic and Molecular Spectroscopy: Basic Aspects and Practical Applications* (Springer, Berlin, Heidelberg 2001) 467
122. G. D. Houser, E. Garmire: Balanced detection technique to measure small changes in transmission, Appl. Opt. **33**, 1059–1062 (1994) 468
123. P. C. D. Hobbs: Ultrasensitive laser measurements without tears, Appl. Opt. **36**, 903–920 (1997) 469
124. M. G. Allen, K. L. Carleton, S. J. Davis, W. J. Kessler, C. E. Otis, D. A. Palombo, D. M. Sonnenfroh: Ultra-sensitive dual beam absorption and gain spectroscopy: Applications for near-IR and visible diode laser sensors, Appl. Opt. **34**, 3240 (1995) 469
125. D. M. Sonnenfroh, W. T. Rawlins, M. G. Allen, C. Gmachl, F. Capasso, A. L. Hutchinson, D. L. Sivco, J. N. Baillargeon, A. Y. Cho: Application of balanced detection to absorption measurements of trace gases with room-temperature, quasi-CW quantum-cascade lasers, Appl. Opt. **40**, 812–820 (2001) 469
126. G. C. Bjorklund: Frequency-modulation spectroscopy: a new method of measuring weak absorption and dispersions, Opt. Lett. **5**, 15 (1980) 470
127. D. E. Cooper, T. F. Gallagher: Double frequency modulation spectroscopy: high modulation frequency with low-bandwidth detectors, Appl. Opt. **24**, 1327 (1985) 470
128. R. Grosskloss, P. Kersten, W. Demtroeder: Sensitive amplitude and phase-modulated absorption spectroscopy with a continuously tunable diode laser, Appl. Phys. B **58**, 137 (1994) 470
129. D. S. Bomse, A. C. Stanton, J. A. Silver: Frequency modulation and wavelength modulation spectroscopies: Comparison of experimental methods using a lead-salt diode laser, Appl. Opt. **31**, 718–731 (1992) 471
130. F. S. Pavone, M. Inguscio: Frequency and wavelength modulation spectroscopties: comparison and experimental methods of using an AlGaAs diode laser, Appl. Phys. B **56**, 118 (1993) 471
131. D. B. Oh, D. C. Hovde: Wavelength modulation detection of acetylene with near-IR external cavity diode laser, Appl. Opt. **34**, 7002–7005 (1995) 471
132. K. Uehara: Dependence of harmonic signals on sample-gas parameters in wavelength-modulation spectroscopy for precise absorption measurements, Appl. Phys. B **67**, 517–523 (1998) 471
133. P. Werle: Laser excess noise and interferometric effects in frequency-modulated diode laser spectrometers, Appl. Phys. B **60**, 499–506 (1995) 471
134. M. S. Zahniser, D. D. Nelson, J. B. McManus, P. Kebabian: Measurement of trace gas fluxes using tunable diode laser spectroscopy, Phil. Trans. R. Soc. London A **351**, 371–382 (1995) 471, 483

135. A. Fried, J. R. Drummond, B. Henry, J. Fox: Versatile integrated tunable diode laser system for high precision: application for ambient measurements of OCS, Appl. Opt. **30**, 1916–1932 (1991) 471
136. T. Iguchi: Modulation waveforms for second-harmonic detection with tunable diode lasers, J. Opt. Soc. Am. B **3**, 419–423 (1986) 471
137. R. G. Pilston, J. U. White: A long path gas absorption cell, J. Opt. Soc. Am. **44**, 572–573 (1954) 472
138. J. U. White: Long optical paths of large aperture, J. Opt. Soc. Am. **32**, 285–288 (1942) 472
139. D. Herriot, H. Kogelnik, R. Kompfner: Off-axis paths in spherical mirror interferometers, Appl. Opt. **3**, 523 (1964) 472
140. S. M. Chernin, E. G. Barskaya: Optical multi-pass matrix systems, Appl. Opt. **30**, 51–58 (1991) 472
141. J. B. McManus, P. L. Kebabian, M. S. Zahniser: Astigmatic mirror multi-pass absorption cells for long-path length spectroscopy, Appl. Opt. **34**, 3336 (1995) 472
142. A. O'Keefe, D. A. G. Deacon: Cavity ring-down optical spectrometer for absorption measurements using pulsed laser sources, Rev. Sci. Instrum. **59**, 2544 (1988) 473, 475
143. J. Lauterbach, D. Kleine, K. Kleinermanns, P. Hering: Cavity-ring-down spectroscopic studies of NO_2 in the region around 613 nm, Appl. Phys. B **71**, 873–876 (2000) 474
144. D. Kleine, S. Stry, J. Lauterbach, K. Kleinermanns, P. Hering: Measurement of the absolute intensity of the fifth CH stretching overtone of benzene using cavity ring-down spectroscopy, Chem. Phys. Lett. **312**, 185–190 (1999) 474
145. G. Berden, R. Peeters, G. Meijer: Cavity ring-down spectroscopy: Experimental schemes and applications, Int. Rev. Phys. Chem. **19**, 565–607 (2000) 475
146. R. Peeters, G. Berden, A. Apituley, G. Meijer: Open-path trace gas detection of ammonia based on cavity-enhanced absorption spectroscopy, Appl. Phys. B **71**, 231–236 (2000) 475
147. R. Peeters, G. Berden, G. Meijer: Sensitive absorption techniques for spectroscopy, Am. Lab. **33**, 60 (2001) 475
148. Y. B. He, B. J. Orr: Rapidly swept, continuous-wave cavity ringdown spectroscopy with optical heterodyne detection, Single- and multi-wavelength sensing of gases, Appl. Phys. B **75**, 267–280 (2002) 475
149. K. K. Lehmann, D. Romanini: The superposition principle and cavity ringdown spectroscopy, J. Chem. Phys. **105**, 10263–10277 (1996) 475
150. B. A. Paldus, J. S. Harris, J. Martin, J. Xie, R. N. Zare: Laser diode cavity ring-down spectroscopy using acousto-optic modulator stabilization, J. Appl. Phys. **82**, 3199–3204 (1997) 475
151. B. A. Paldus, C. C. Harb, T. G. Spence, B. Wilke, J. Xie, J. S. Harris, R. N. Zare: Cavity-locked ring-down spectroscopy, J. Appl. Phys. **83**, 3991–3997 (1998) 475
152. J. J. Scherer, J. B. Paul, A. O'Keefe, R. J. Saykally: Cavity ringdown laser absorption spectroscopy, Chem. Rev. **97**, 25–51 (1997) 475
153. R. A. Provencal, J. B. Paul, E. Michael, R. J. Saykally: Absorption spectroscopy technique provides extremely high sensitivity, Photon. Spectra **32**, 159 ff. (1998) 475
154. J. B. Paul, R. J. Saykally: Cavity ring-down laser absorption spectroscopy, Anal. Chem. **69**, A287–A292 (1997) 475

155. K. W. Busch, M. A. Busch: *Cavity Ring-Down Spectroscopy, An Ultratrace-Absorption Measurement Technique* (American Chemical Society, Washington, DC 1999) 475
156. J. J. Scherer, D. Voelkel, D. J. Rakestraw, J. B. Paul, C. P. Collier, A. O'Keefe, R. J. Saykally: Infrared Cavity Ringdown Laser Absorption Spectroscopy (IR-CRLAS), Chem. Phys. Lett. **245**, 273–280 (1995) 475, 476
157. K. K. Lehmann: Ring-down cavity spectroscopy cell using continuous wave excitation for trace species detection, US patent no. 5,528,040 (1996) 476
158. D. Romanini, A. A. Kachanov, N. Sadeghi, F. Stoeckel: CW cavity ring down spectroscopy, Chem. Phys. Lett. **264**, 316–322 (1997) 476
159. D. Romanini, A. A. Kachanov, F. Stoeckel: Diode laser cavity ring down spectroscopy, Chem. Phys. Lett. **270**, 538–545 (1997) 476
160. B. A. Paldus, C. C. Harb, T. G. Spence, R. N. Zare, C. Gmachl, F. Capasso, D. L. Sivco, J. N. Baillargeon, A. L. Hutchinson, A. Y. Cho: Cavity ring-down spectroscopy using mid-infrared quantum-cascade lasers, Opt. Lett. **25**, 666–668 (2000) 476, 487
161. A. A. Kosterev, A. L. Malinovsky, F. K. Tittel, C. Gmachl, F. Capasso, D. L. Sivco, J. N. Baillargeon, A. L. Hutchinson, A. Y. Cho: Cavity ring-down spectroscopic detection of nitric oxide with a continuous-wave quantum-cascade laser, Appl. Opt. **40**, 5522–5529 (2001) 476, 486, 487
162. K. W. Aniolek, P. E. Powers, T. J. Kulp, B. A. Richman, S. E. Bisson: Cavity ring-down laser absorption spectroscopy with a 1 kHz mid-infrared periodically poled lithium niobate optical parametric generator optical parametric amplifier, Chem. Phys. Lett. **302**, 555–562 (1999) 476
163. R. J. Saykally, R. Casaes: Cavity ring-down technique measures absorption, Laser Focus World **37**, 159–162 (2001) 476
164. A. O'Keefe: Integrated cavity output analysis of ultra-weak absorption, Chem. Phys. Lett. **293**, 331–336 (1998) 476
165. R. Engeln, G. Vonhelden, G. Berden, G. Meijer: Phase shift cavity ring down absorption spectroscopy, Chem. Phys. Lett. **262**, 105–109 (1996) 476
166. R. Engeln, G. Berden, R. Peeters, G. Meijer: Cavity enhanced absorption and cavity enhanced magnetic rotation spectroscopy, Rev. Sci. Instrum. **69**, 3763–3769 (1998) 476
167. J. B. Paul, L. Lapson, J. G. Anderson: Ultrasensitive absorption spectroscopy with a high-finesse optical cavity and off-axis alignment, Appl. Opt. **40**, 4904–4910 (2001) 476, 477, 486
168. M. Murtz, B. Frech, W. Urban: High-resolution cavity leak-out absorption spectroscopy in the 10-μm region, Appl. Phys. B **68**, 243–249 (1999) 476
169. L. Menzel, A. A. Kosterev, R. F. Curl, F. K. Tittel, C. Gmachl, F. Capasso, D. L. Sivco, J. N. Baillargeon, A. L. Hutchinson, A. Y. Cho, W. Urban: Spectroscopic detection of biological NO with a quantum cascade laser, Appl. Phys. B **72**, 859–863 (2001) 476, 486
170. D. S. Baer, J. B. Paul, M. Gupta, A. O'Keefe: Sensitive absorption measurements in the near-infrared region using off-axis integrated cavity output spectroscopy, Appl. Phys. B **75**, 261–265 (2002) 477
171. L. S. Ma, J. Ye, P. Dube, J. L. Hall: Ultrasensitive frequency-modulation spectroscopy enhanced by a high-finesse optical cavity: Theory and application to overtone transitions of C_2H_2 and C_2HD, J. Opt. Soc. Am. B **16**, 2255–2268 (1999) 477

172. J. Ye, L. S. Ma, J. L. Hall: Sub-doppler optical frequency reference at 1.064-μm by means of ultrasensitive cavity-enhanced frequency modulation spectroscopy of a C_2HD overtone transition, Opt. Lett. **21**, 1000–1002 (1996) 477
173. M. S. Taubman, R. M. Williams, T. L. Myers, F. Capasso, C. Gmachl, D. L. Sivco, A. L. Hutchinson, A. Y. Cho: Sub-Doppler NICE-OHMS spectroscopy at 8.5 microns using a quantum cascade laser, in OSA Trends in Optics and Photonics (TOPS) Vol 73, Conference on Lasers and Electro-Optics, OSA Technical Digest (Opt. Soc. of Am., Washington, DC., 2002) pp.625–626 478
174. M. A. Moeckli, C. Hilbes, M. W. Sigrist: Photoacoustic multicomponent gas analysis using a Levenberg–Marquardt fitting algorithm, Appl. Phys. B **67**, 449–458 (1998) 478
175. J. Oomens, H. Zuckermann, S. Persijn, D. H. Parker, F. J. M. Harren: CO-laser-based photoacoustic trace-gas detection – applications in postharvest physiology, Appl. Phys. B **67**, 459–466 (1998) 478
176. M. A. Moeckli, M. Fierz, M. W. Sigrist: Emission factors for ethene and ammonia from a tunnel study with a photoacoustic trace gas detection system, Environ. Sci. Technol. **30**, 2864–2867 (1996) 478
177. M. Nagele, M. W. Sigrist: Mobile laser spectrometer with novel resonant multipass photoacoustic cell for trace-gas sensing, Appl. Phys. B **70**, 895–901 (2000) 478
178. B. G. Ageev, Y. N. Ponomarev, V. A. Sapozhnikova: Laser photoacoustic spectroscopy of biosystems gas exchange with the atmosphere, Appl. Phys. B **67**, 467–473 (1998) 478
179. F. J. M. Harren, G. Cotti, J. Oomens, S. L. Hekkert: Photoacoustic spectroscopy in trace gas monitoring, in *Encyclopedia of Analytical Chemistry*, R. A. Meyers (Ed.) (Wiley, Chichester 2000) pp. 2203–2226 478
180. A. Bohren, M. W. Sigrist: Optical parametric oscillator based difference frequency laser source for photoacoustic trace gas spectroscopy in the 3-μm mid-IR range, Infrared Phys. Technol. **38**, 423–435 (1997) 478
181. Z. Bozoki, J. Sneider, Z. Gingl, A. Mohacsi, M. Szakall, Z. Bor, G. Szabo: A high-sensitivity, near-infrared tunable-diode-laser-based photoacoustic water-vapour-detection system for automated operation, Measurement Sci. Technol. **10**, 999–1003 (1999) 478
182. F. G. C. Bijnen, F. J. M. Harren, J. H. P. Hackstein, J. Reuss: Intracavity CO laser photoacoustic trace gas detection – cyclic CH_4, H_2O and CO_2 emission by cockroaches and scarab beetles, Appl. Opt. **35**, 5357–5368 (1996) 478
183. V. A. Kapitanov, Y. U. N. Ponomarev, K. Song, H. K. Cha, J. Lee: Resonance photoacoustic spectroscopy and gas analysis of gaseous flow at reduced pressure, Appl. Phys. B **73**, 745–750 (2001) 478
184. M. B. Pushkarsky, M. E. Webber, O. Baghdassarian, L. R. Narasimhan, C. K. N. Patel: Laser-based photoacoustic ammonia sensors for industrial applications, Appl. Phys. B **75**, 391–396 (2002) 479
185. A. Schmohl, A. Miklos, P. Hess: Detection of ammonia by photoacoustic spectroscopy with semiconductor lasers, Appl. Opt. **41**, 1815–1823 (2002) 479
186. A. A. Kosterev, Y. A. Bakhirkin, R. F.Curl, F. K. Tittel: Quartz-enhanced photoacoustic spectroscopy, Opt. Lett. **27**, 1902–1904 (2002) 479
187. A. Fried, W. W. Berg: Photoacoustic detection of HCl, Opt. Lett. **8**, 160–162 (1983) 479

188. M. Avery-Owens, C. C. Davis, R. R. Dickerson: A photothermal interferometer for gas-phase ammonia detection, Anal. Chem. **71**, 1391–1399 (1999) 479
189. B. A. Paldus, T. G. Spence, R. N. Zare, J. Oomens, F. J. M. Harren, D. H. Parker, C. Gmachl, F. Cappasso, D. L. Sivco, J. N. Baillargeon, A. L. Hutchinson, A. Y. Cho: Photoacoustic spectroscopy using quantum-cascade lasers, Opt. Lett. **24**, 178–180 (1999) 480
190. D. Hofstetter, M. Beck, J. Faist, M. Nagele, M. W. Sigrist: Photoacoustic spectroscopy with quantum cascade distributed-feedback lasers, Opt. Lett. **26**, 887–889 (2001) 480
191. P. Werle, R. Mucke, F. Slemr: The limits of signal averaging in atmospheric trace-gas monitoring by tunable diode-laser absorption spectroscopy (TDLAS), Appl. Phys. B **57**, 131–139 (1993) 483, 484
192. S. Sewell, A. Fried, B. Henry, J. R. Drummond: A field diode laser spectrometer employing an astigmatic Herriott cell, in *Tunable Diode Laser Spectroscopy, Lidar, and DIAL Techniques for Environmental and Industrial Measurements*, A. Fried, D. K. Killinger, H. I. Schiff (Eds.) (SPIE, Atlanta, GA 1993) pp. 72–80 484
193. A. Fried, B. P. Wert, J. G. Walega, D. Richter, W. T. Potter: Airborne measurements of formaldehyde employing a high-performance tunable diode laser absorptoion system, in *Diode Lasers and Applications in Atmospheric Sensing*, A. Fried (Ed.), Proc. SPIE **4817**, 177–183 (2002) 484
194. R. W. Waynant, I. K. Ilev, I. Gannot: Mid-infrared laser applications in medicine and biology, Phil. Trans. R. Soc. London A 635–644 (2001) 486
195. P. Murtz, L. Menzel, W. Bloch, A. Hess, O. Michel, W. Urban: LMR spectroscopy: a new sensitive method for on-line recording of nitric oxide in breath, J. Appl. Physiol. **86**, 1075–1080 (1999) 486
196. H. Dahnke, D. Kleine, P. Hering, M. Murtz: Real-time monitoring of ethane in human breath using mid-infrared cavity leak-out spectroscopy, Appl. Phys. B **72**, 971–975 (2001) 486
197. D. E. Cooper, R. U. Martinelli, C. B. Carlisle, H. Riris, D. B. Bour, R. J. Menna: Measurements of $^{12}CO_2$:$^{13}CO_2$ ratios for medical diagnostics with 1.6-micron distributed-feedback semiconductor diode lasers, Appl. Opt. **32**, 6727–6731 (1993) 486
198. L. R. Narasimhan, W. Goodman, C. K. N. Patel: Correlation of breath ammonia with blood urea nitrogen and creatinine during hemodialysis, Proc. National Acad. Sci. United States Am. **98**, 4617–4621 (2001) 486
199. C. Roller, K. Namjou, J. D. Jeffers, M. Camp. A. Mock, P. J. McCann, J. Grego: Nitric oxide breath testing by tunable-diode laser absorption spectroscopy, Application in monitoring respiratory inflammation, Appl. Opt. **41**, 6018–6029 (2002) 486
200. I. Tsujino, M. Nishimura, A. Kamachi, H. Makita, M. Munakata, K. Miyamoto, Y. Kawakami: Exhaled nitric oxide – Is it really a good marker of airway inflammation in bronchial asthma?, Respiration **67**, 645–651 (2000) 486
201. T. Ingi, J. Cheng, G. V. Ronnett: Carbon monoxide – an endogenous modulator of the nitric oxide-cyclic GMP signaling system, Neuron **16**, 835–842 (1996) 489
202. Y. Morimoto, W. Durante, D. G. Lancaster, J. Klattenhoff, F. K. Tittel: Real-time measurements of endogenous CO production from vascular cells using an ultrasensitive laser sensor, Am. J. Physiol. **280**, H483–H488 (2001) 489, 490

203. A. A. Kosterev, F. K. Tittel, W. Durante, M. Allen, R. Köhler, C. Gmachl, F. Capasso, D. L. Sivco, A. Y. Cho: Detection of biogenic CO production above vascular cell cultures using a near-room temperature QC-DFB laser, Appl. Phys. B **74**, 95–99 (2002) 489
204. A. A. Kosterev, F. K. Tittel, R. Köhler, C. Gmachl, F. Capasso, D. L. Sivco, A. Y. Cho, S. Wehe, M. G. Allen: Thermoelectrically cooled quantum-cascade-laser-based sensor for the continuous monitoring of ambient atmospheric carbon monoxide, Appl. Opt. **41**, 1169–1173 (2002) 489
205. A. A. Kosterev, R. F. Curl, F. K. Tittel, R. Köhler, C. Gmachl, F. Capasso, D. L. Sivco, A. Y. Cho: Transported automated ammonia sensor based on a pulsed thermoelectrically cooled QC-DFB laser, Appl. Opt. **41**, 573–578 (2002) 490
206. A. A.Kosterev, F. K. Tittel: Chemical sensorsbased on quantum cascade lasers, IEEE Quant. Electron. **38**, 582–591 (2002) 490
207. D. Richter: Portable mid-infrared gas sensors: development and applications, Dissertation, Rice University, Houston (2001) 491
208. D. Richter, A. Fried, B. P. Wert, J. G. Walega, F. K. Tittel: Development of a tunable mid-IR difference-frequency laser source for highly sensitive airborne trace gas detection, Appl. Phys. B **75**, 281–288 (2002) 491, 493
209. D. Richter, M. Erdelyi, R. F. Curl, F. K. Tittel, C. Oppenheimer, H. J. Duffell, M. Burton: Field measurements of volcanic gases using tunable diode laser based mid-infrared and Fourier transform infrared spectrometers, Opt. Lasers Engin. **37**, 171–186 (2002) 492
210. D. Richter, F. K. Tittel, J. A. Bahr, D. T. Wickham, J. D. Wright, J. C. Graf: Diode laser based formaldehyde measurements in a catalytic trace contaminant control system, paper 2302, Proc. 30th Int. Conf. Environmental Systems (ICES), Toulouse, France (2000) 492
211. D. Rehle, D. Leleux, M. Erdelyi, F. Tittel, M. Fraser, S. Friedfeld: Ambient formaldehyde detection with a laser spectrometer based on difference-frequency generation in PPLN, Appl. Phys. B **72**, 947–952 (2001) 492
212. D. Richter, A. Fried, G. S. Tyndall, E. Oteiza, M. Erdelyi, F. K. Tittel: Tunable telecom diode laser based mid-IR source at 2.64 microns, OSA Trends Optics Photonics, Advanced Solid State Lasers **68**, 351–353 (2002) 494
213. P. Bergamaschi, M. Schupp, G. W. Harris: High-precision direct measurements of $^{13}CH_4/^{12}CH_4$ and $^{12}CH_3D/^{12}CH_4$ ratios in atmospheric methane sources by means of a long-path tunable diode laser absorption spectrometer, Appl. Opt. **33**, 7704–7716 (1994) 495, 496
214. M. Erdelyi, D. Richter, F. K. Tittel: Measurement of $^{13}CO_2$ / $^{12}CO_2$ isotopic ratio using a difference-frequency-based sensor operating at 4.35 µm, Appl. Phys. B **75**, 289–295 (2002) 495
215. J. B. McManus, M. S. Zahniser, D. D. Nelson, L. R. Williams, C. E. Kolb: Infrared laser spectrometer with balanced absorption for measurement of isotopic ratios of carbon isotopes, Spectrochim. Acta A **58**, 2465–2479 (2002) 496
216. E. R. T. Kerstel, R. v. Trigt, N. Dam, J. Reuss, H. A. J. Meijer: Simultaneous determination of the H-2/H-1, O-17/O-16, and O-18/O-16 isotope abundance ratios in water by means of laser spectrometry, Anal. Chem. **71**, 5297–5303 (1999) 496

217. K. Uehara, K. Yamamoto, T. Kikugawa, N. Yoshida: Isotope analysis of environmental substances by a new laser-spectroscopic method utilizing different pathlengths, Sensors Actuators B **74**, 173–178 (2001) 496
218. E. R. Crosson, K. N. Ricci, B. A. Richman, F. C. Chilese, T. G. Owano, R. A. Provencal, M. W. Todd, J. Glasser, Alex A. Kachanov, B. A. Paldus, T. G. Spence, R. N. Zare: Stable isotope ratios using cavity ring-down spectroscopy: determination of ^{13}C / ^{12}C for carbon dioxide in human breath, Anal. Chem. **74**, 2003–2007 (2002) 496
219. L. Hvozdara, N. Pennington, M. Kraft, M. Karlowatz, B. Mizaikoff: Quantum cascade lasers for mid-infrared spectroscopy, Vibr. Spectrosc. **30**, 53–58 (2002) 496
220. D. Richter, A. Fried, F. K. Tittel: Special Issue: Trends in laser sources, spectroscopic techniques and their applications to trace gas detection, Appl. Phys. B **75**, 143–403 (2002) 496
221. R. F. Curl, F. K. Tittel: Tunable Infrared Laser Spectroscopy, Ann. Rep. Progr. Chem. C **98**, 217–270 (2002) 496

Index